Assessment of pluriannual and decadal changes in terrestrial water storage predicted by global hydrological models in comparison with GRACE satellite gravity mission

Julia Pfeffer[1], Anny Cazenave[1,2], Alejandro Blazquez[2,3], Bertrand Decharme[4], Simon Munier[4], Anne Barnoud[1]

[1] Magellium, Ramonville-Saint-Agne, 31520, France
[2] LEGOS, Université de Toulouse, Toulouse, 31400, France
[3] CNES, Toulouse, 31400, France
[4] CNRM/Météo France/CNRS, Toulouse, 31057, France

Correspondence to: Julia Pfeffer (julia.pfeffer@magellium.fr)

Abstract. The GRACE (Gravity Recovery And Climate Experiment) satellite gravity mission enables global monitoring of the mass transport within the Earth's system, leading to unprecedented advances in our understanding of the global water cycle in a changing climate. This study focuses on the quantification of changes in terrestrial water storage based on an ensemble of GRACE solutions and two global hydrological models. Significant changes in terrestrial water storage are detected at pluriannual and decadal time-scales in GRACE satellite gravity data, that are generally underestimated by global hydrological models. The largest differences (more than 20 cm in equivalent water height) are observed in South America (Amazon, Sao Francisco and Parana river basins) and tropical Africa (Congo, Zambezi and Okavango river basins). Significant differences (a few cm) are observed worldwide at similar time-scales, and are generally well correlated with precipitation. While the origin of such differences is unknown, part of it is likely to be climate-related and at least partially due to inaccurate predictions of hydrological models. Pluri-annual to decadal changes in the terrestrial water cycle may indeed be overlooked in global hydrological models due to inaccurate meteorological forcing (e.g., precipitation), unresolved groundwater processes, anthropogenic influences, changing vegetation cover and limited calibration/validation datasets. Significant differences between GRACE satellite measurements and hydrological model predictions have been identified, quantified and characterised in the present study. Efforts must be made to better understand the gap between both methods at pluriannual and decadal time-scales, which challenges the use of global hydrological models for the prediction of the evolution of water resources in changing climate conditions.

Deleted: Detection of slow
Deleted: and GRACE-FO
Deleted: s
Deleted: and GRACE Follow-On (FO)
Deleted: s
Deleted: and GRACE-FO
Deleted: and GRACE-FO
Deleted: Slow

1 Introduction

The GRACE (Gravity Recovery And Climate Experiment; Tapley et al., 2004) and GRACE Follow-On (GRACE-FO; Landerer et al., 2020) missions provide spatio-temporal observations of the gravity field spanning over two decades, sensitive to the redistribution of masses from the deep Earth's interior to the top of the atmosphere (e.g., Chen et al., 2022). The GRACE and GRACE-FO satellite observations have been widely used to estimate changes in terrestrial water storage (TWS), expressed in equivalent water heights, representing changes in surface density (i.e. changes in mass per unit area) modelled as a layer of water of variable thickness in space and time (e.g., Wahr et al., 1998). Changes in TWS range from a few millimetres to a few ten centimetres from arid (e.g., deserts) to humid (e.g., tropical rain forests) regions of the world, and are dominated first by seasonal changes, then by long-term changes including both linear trends and interannual variability (e.g., Humphrey et al., 2016). Locally (mostly along the Amazon River), seasonal TWS variations can reach up to 1 or 2 metres. Decadal trends in TWS have been attributed to climate variability (e.g., change in precipitation), direct human impacts (e.g., irrigation) and the combination of both effects (Rodell et al., 2018). Significant groundwater depletion has for example been observed in the Central Valley (California), in response to two extreme and prolonged droughts intensified by groundwater pumping for agriculture, wetland management and domestic use (e.g., Scanlon et al., 2012; Ohja et al., 2018).

Trends in TWS are often temporary due to climate variability (e.g., Alam et al., 2021) and changes in water consumption policies (e.g., Bhanja et al., 2017). Significant interannual TWS variations detected in large river basins have been attributed to a combination of eight major climate modes, including the El Niño-Southern Oscillation (ENSO), Pacific Decadal Oscillation, North Atlantic Oscillation, Atlantic Multidecadal Oscillation and Southern Annular Mode (e.g., Pfeffer et al., 2022). Successive droughts and floods events have been associated with a succession of positive (El Niño) and negative (La Niña) phases of ENSO in various regions of the world, such as Australia, Southern Africa or parts of the Amazon River basin (e.g., Ni et al., 2018, Anyah et al., 2018, Xie et al., 2019). Drought (e.g., Thomas et al., 2017) and flood potential (e.g., Sun et al., 2017) indices using GRACE observations have been developed to monitor the impact of extreme events on freshwater resources, taking into account all climatic and anthropogenic mechanisms and all water reservoirs from the surface to deep aquifers.

Beyond monitoring the TWS variability, GRACE data have widely been used to constrain poorly observed components of the water mass balance. Typically, TWS changes (dTWS/dt) can be expressed as:

$$\frac{dTWS}{dt} = P - ET - R \qquad (1)$$

and used to constrain the terrestrial water discharge (R) based on independent estimates of the net precipitation (precipitation P minus evapotranspiration ET), with good agreement with available in situ river gauges (e.g., Syed et al., 2009 and 2010). Alternatively, groundwater storage (GWS) variations can be estimated as the difference between the TWS changes estimated

Deleted: mass anomalies

Deleted: located at the Earth's surface

Deleted: decadal

Deleted: Multidecadal

Deleted: and GRACE-FO

Deleted: and GRACE-FO

from GRACE observations and ice, snow, surface water and soil moisture variations estimated from independent data sources (e.g., Chen et al., 2016; Frappart et al., 2018). These approaches often rely on global hydrological models, land surface models or land surface reanalyses, to estimate one or several terms of the water mass balance equation, assuming that the water fluxes (e.g., net precipitation, see for example Chandanpurkar et al., 2017) and water storage anomalies from the ice, snow, surface and soil reservoirs (e.g., Rodell et al., 2007; Bhanja et al., 2016; Thomas and Famiglietti, 2019; Frappart et al., 2019) are modelled with sufficient accuracy, so that the residual gravity signal can be attributed to the variable of interest (i.e. terrestrial freshwater discharge or GWS changes).

If the spatial and temporal variability of TWS is generally well captured, global hydrological models and land surface models tend to underestimate the amplitude of seasonal signals (e.g., Döll et al., 2014) and decadal trends (e.g., Scanlon et al., 2018) when compared to GRACE observations. The differences in TWS between satellite gravity observations and model predictions have been shown to depend on the choice of models and river basin considered (e.g., Döll et al., 2014; Wada et al., 2014; Scanlon et al., 2018; Scanlon et al., 2019; Decharme et al., 2019; Yang et al., 2020 and Felfelani et al., 2017). Seasonal changes in TWS are often underestimated by hydrological and land surface models in tropical, arid and semi-arid basins, and overestimated at higher latitudes in the Northern hemisphere, likely due to insufficient surface and ground water storage estimates in tropical basins, and to a misrepresentation of evapotranspiration and snow physics at higher latitudes (Scanlon et al., 2019). Some models lead to better performance in heavily managed river basins and, on the contrary, to erroneous trends and seasonal cycles in regions where the natural variability is dominant (e.g., Wada et al., 2014; Scanlon et al., 2019; Felfelani et al., 2017). The performance of models also varies during the recharge and discharge periods, suggesting that some processes (e.g., reservoir operation) may be adequately captured by a model, while other processes (e.g., groundwater dynamics) may be overlooked (Felfelani et al., 2017). The reasons for discrepancies between models and satellite gravity observations remain largely unknown, though improvements in the parameterization of global hydrological and land surface models are often recommended to reliably predict spatial and temporal changes in TWS, especially regarding aquifers (e.g., Decharme et al., 2019, Scanlon et al., 2019, Felfelani et al., 2017).

This study focuses on the comparison of two global hydrological models, ISBA-CTRIP (Decharme et al., 2019) and WGHM (Müller Schmied et al., 2021), against GRACE-based TWS observations at interannual and decadal time-scales. These two models have been chosen, because they provide a very precise representation of hydrological processes in natural (ISBA-CTRIP) and anthropized (WGHM) environments. Besides, both models have been widely used by the scientific community. In particular, ISBA-CTRIP is contributing to the Coupled Model Intercomparison Project CMIP6 (Voldoire et al., 2019), and WGHM to the Inter-Sectoral Impact Model Intercomparison Project (ISIMIP; Herbert and Döll, 2019). While the seasonal variations in TWS have been extensively studied (e.g., Döll et al., 2014; Wada et al., 2014; Scanlon et al., 2019; Decharme et al., 2019 and Felfelani et al., 2017), little attention has been paid to longer time-scales, often only estimated as linear trends (Scanlon et al., 2018; Felfelani et al., 2017). Significant non-linear variability occurs however at interannual time-scales, that

Deleted: and GRACE-FO

may lead to considerable stress on water resources and large uncertainties on climate model projections. Besides, the same model may have different performances at seasonal, interannual and decadal time-scales, as different processes prevail at such different time scales (e.g., Scanlon et al., 2018, Scanlon et al., 2019; Felfelani et al., 2017). This study will therefore quantify and characterise the amplitude of TWS at interannual and decadal time-scales for 9 GRACE solutions (3 mascon solutions and 6 spherical harmonic solutions) and 2 global hydrological models between April 2002 and December 2016.

Deleted: The differences in TWS will be compared to the dispersion in GRACE solution to evaluate their significance and to precipitation to better understand their origin. Such assessment will allow evaluating the performance of hydrological models used in CMIP6 (e.g., Voldoire et al., 2019) projections, ISI-MIP (e.g., Herbert & Döll, 2019) projections and in value-added products based on a synergy of satellite data and models.

2 Methods

2.1 Satellite gravity data

Total terrestrial water storage (TWS) changes have been estimated using the latest release of three mascon solutions from the JPL (RL06 Version 02, Wiese et a., 2019), CSR (RL06 V02; Save et al., 2016 and Save, 2020) and GSFC (RL06 V01, Loomis et al., 2019a) and six solutions based on spherical harmonic coefficients of the gravitational potential from the JPL (RL06, GRACE-FO, 2019a; Yuan, 2019), CSR (RL06, GRACE-FO, 2019b; Yuan, 2019), GFZ (RL06, Dahle et al., 2018), ITSG (GRACE2018, Mayer-Gürr et al., 2018), COST-G (RL01, Meyer et al., 2020) and CNES-GRGS (RL05, Lemoine and Bourgogne, 2020). The same corrections for the geocenter (Sun et al., 2016), C_{20} coefficients (Loomis et al., 2019b) and GIA (ICE6G-D by Peltier et al., (2018)) have been applied for mascon and spherical harmonic solutions. The Stokes coefficients from the JPL, CSR, GFZ, ITSG, COST-G and CNES-GRGS solutions, with the aforementioned corrections applied, have been truncated at degree 60, converted to surface mass anomalies expressed as equivalent water height (cm) and projected on the WGS84 ellipsoid using the locally spherical approximation (eq. 27 in Ditmar et al., 2018) implemented in the l3py python package (Akvas, 2018). Systematic errors (i.e., stripes) have been removed from spherical harmonic solutions (except for the constrained CNES-GRGS solutions) using an anisotropic filter based on the principle of diffusion (Goux et al., 2022), using Daley length scales of 200 and 300 km in the North-South and East-West directions, and a shape of Matern function close to a Gaussian (8 iterations). The diffusive filter allows the conservation of mass within the continental domain, defined here as grid cells where at least 30% of the altitudes from ETOPO1 Global Relief Model (NOAA National Geophysical Data Center, 2009) are above sea level. Small islands (<100 000 km^2) have been excluded from the continental domain, because of the limited spatial resolution of monthly GRACE products (a few hundred kilometres). By default, the GRACE-derived TWS anomalies used in this study is the average of the nine processed GRACE solutions. The uncertainty on GRACE-based TWS anomalies is estimated as the dispersion (minimum to maximum) between the 9 GRACE solutions.

2.2 Global hydrological models

Total terrestrial water storage (TWS) TWS changes have also been estimated using the ISBA-CTRIP (Interaction Soil Biosphere Atmosphere - CNRM (Centre National de Recherches Météorologiques) version of Total Runoff Integrating Pathways) global land surface modelling system (Decharme et al., 2019) and the version 2.2d (Müller Schmied et al., 2021) of the WaterGap Global Hydrological Model (WGHM) including glaciers.

ISBA solves the water and energy balance in the soil, canopy, snow and surface water bodies, and CTRIP simulates discharges through the global river network, as well as the dynamic of both the seasonal floodplains and the unconfined aquifers. ISBA and CTRIP are coupled through the land surface interface SURFEX, allowing complex interactions (e.g., floodplain freewater evaporation, and upwards capillarity fluxes between groundwaters and superficial soils) between the atmosphere, land surface, soil and aquifer. ISBA-CTRIP is forced at a 3-hourly timestep with the ERA-Interim atmospheric reanalysis (Dee et al., 2011) for air temperature and humidity, wind speed, surface pressure and total radiative fluxes, and with the gauge-based Global Precipitation Climatology Center (GPCC) Full Data Product V6 (Schneider et al., 2014) for precipitation.

WGHM 2.2d simulates changes in water flows and storage using a vertical mass balance for the canopy, snow and soil and a lateral mass balance for the surface water bodies and groundwater (Müller Schmied et al., 2021). WGHM is coupled with a global water use model, taking into account water impoundment in artificial reservoirs and regulated lakes and water withdrawals for irrigation, livestock, domestic use, manufacturing and thermal power (Müller Schmied et al., 2021). Anthropogenic water withdrawals/impoundments are assumed to only impact surface waters and groundwaters (Müller Schmied et al., 2021). In addition, water storage changes in continental glaciers have been simulated with the Global Glacier Model (Marzeion et al., 2012) and added as an input to WaterGap (Caceres et al., 2022). The WGHM uses meteorological input data from WFDEI (Weedon et al., 2014) also based on the ERA-Interim atmospheric reanalysis for air temperature and solar radiation and GPCC for precipitation. Two model variants are available using different irrigation efficiencies (optimal and 70% of optimal) (Döll et al., 2014b). Both being equally plausible given the limited datasets available to characterise groundwater abstractions for irrigation, we averaged the two variants in the present study.

2.3 Lake data

Lake water storage anomalies have then been added to the predicted TWS anomalies from ISBA-CTRIP and WGHM. Indeed, although WGHM2.2d includes artificial and natural lakes in its framework, large differences were observed between the observed and predicted TWS anomalies around large lakes (e.g., American and African Great Lakes, Caspian Sea, Volta Lake), that were greatly reduced with the application of a lake correction (Appendix A).

Changes in lake volume were estimated for 100 lakes during the whole GRACE period from the hydroweb database (https://hydroweb.theia-land.fr/), based on a combination of lake level measurements from satellite altimetry and lake area measurements from satellite imagery (e.g., Cretaux et al., 2016). Then lake volume changes are converted into equivalent water heights (m) over a regular 1x1 degree grid, using the GLWD (Global Lakes and Wetlands Database) shapes for lakes larger than 5000 km^2 as detailed in Blazquez et al. (in preparation).

2.4 Precipitation data

Precipitation is estimated using the gauge-based Global Precipitation Climatology Center (GPCC) Full Data Product V6 (Schneider et al., 2014) and the IMERG (Integrated Multi-satellitE Retrievals for GPM) data product (Huffman et al., 2019) based on the TRMM (Tropical Rainfall Measuring Mission: 2000-2015) and GPM (Global Precipitation Measurement: 2014 - present) satellite data.

2.5 Data processing

The period of common availability for all datasets spans from April 2002 (first estimation of TWS changes with GRACE data) to December 2016 (latest estimation of TWS changes with WGHM data). All time-series have been averaged monthly. Months with missing data are excluded from all datasets, leaving 141 valid months between April 2002 and December 2016. All dataset were interpolated to a regular 1°x1° grid using the conservative algorithm from xESMF (Zhuang et al., 2020), allowing to preserve the integral of the surface mass anomalies across the grid conversion (i.e., the water mass anomaly over a 1°x1° grid cell is equal to the area-weighted average of the mass anomalies from overlapping cells in the source grid). Because this study focuses on interannual to decadal changes in total terrestrial water storage, regions where observed mass changes are known to be dominated by other processes have been masked. These include the oceans, ice-covered regions such as Antarctica, Greenland, Arctic islands, and regions impacted by very large earthquakes (Sumatra, Tohoku, Maule) defined by Tang et al. (2020). Seasonal signals have been removed by least-squares adjustment of annual and semi-annual sinusoids. Finally, to be able to compare higher-resolution hydrology products to GRACE-based TWS anomalies, a diffusive filter with an isotropic Daley length of 250 km has been applied to all products. In the following, we refer to the fully processed time-series as TWS anomalies. Residual TWS anomalies (sometimes shortened as residuals) refer to the difference between the TWS anomalies estimated with the average GRACE solution and the TWS anomalies estimated with one of the two global hydrological models considered in this study (either ISBA-CTRIP or WGHM). The amplitude of the interannual variability is expressed as the range at 95% CL of fully processed TWS anomalies. The range at 95% CL is defined as the difference between the 97.5 and 2.5 percentiles. It provides a more accurate quantification of the amplitude of the non-seasonal TWS variations than the RMS, while allowing the removal of extreme values.

Deleted: .

3 Results

3.1 Comparison of observed and predicted TWS anomalies

TWS anomalies are globally lower in hydrological models than in GRACE solutions, leaving large residuals in GRACE satellite data (Fig. 1). The underestimation of TWS anomalies is more acute with WGHM (Fig. 1d) than with ISBA (Fig. 1c).

Deleted: (Fig. 1)

Deleted: (Fig. 1c and d)

Deleted: (Fig. 1a)

Deleted: e and f

Significant (> 5 cm) residual TWS anomalies (Fig. 1e and f) are observed in South America (Amazon, Orinoco, Sao Francisco and Parana river basins), Africa (Congo and Zambezi basins), Australia (northern part of the continent), Eurasia (India, North European Plains, Ural Mountains, Siberian Plateau) and North America (Colorado Plateau, Rocky Mountains). All GRACE solutions are remarkably consistent one with another, which is evidenced by small dispersion values (Fig 1b). The amplitude of non-seasonal TWS signals is very similar in mascons and spherical harmonic solutions, which is generally larger than in global hydrological models (supplementary material Fig. S1 and S2).

In most regions of the world, the differences between GRACE and global hydrological models (Fig. 1e and f) are much larger than the dispersion between the different GRACE solutions. Indeed, the residual TWS anomalies are significantly larger (5th, 50th and 95th percentiles of the RMS of residual TWS anomalies at 4, 8 and 20 cm) than the uncertainty on GRACE data estimated by the dispersion among the 9 solutions (5th, 50th and 95th percentiles of the standard deviation between the 9 GRACE solutions at 1, 3 and 13 cm). The largest (≥ 5 cm) dispersion values are observed in coastal and mountainous regions, or in regions with very large (≥ 20 cm) residuals (Fig. 1b). Larger sources of errors are indeed expected near the coast in GRACE measurements due to leakage errors, making the interpretation of residual signals difficult in islands such as Madagascar or the Indonesian Archipelago. Similarly significant ice-melt from glaciers occurs in mountainous regions such as the Alaska or Tibetan plateau, which is monitored by GRACE but not simulated by global hydrological models, leaving large TWS residuals (≳ 30 cm) around glaciers. Global hydrological models should therefore not be compared with GRACE around glaciers, whose limits have been determined with the sixth version of the Randolph Glacier Inventory (RGI Consortium, 2017) identified with white contours in Fig. 1.

To be able to differentiate a systematic underestimation of TWS anomalies from singular differences in the spatial and temporal variability, we computed the range ratio between the average GRACE solution and each hydrological model. For most regions of the world (Fig. 2a and 2b), the range of TWS anomalies is larger for GRACE than for ISBA-CTRIP or WGHM, except in East Canada (Ontario, Quebec, Newfoundland), North Asia (East Siberia, Ob River, Finland/Northwest Russia) and central Africa (Cameroun, Gabon, Congo). In these regions, the coefficient of determination (R^2) between the GRACE and the hydrological models is typically negative (Fig. 2c and d), indicating that the variance of the residuals is larger than the variance of GRACE data. The global hydrological models ISBA-CTRIP and WGHM are therefore not able to predict the TWS variability estimated from GRACE satellite data in these regions.

Deleted: Very large (≥ 30 cm) residual TWS anomalies are observed around glaciers (Alaska, Patagonia) due to ice-melting, which is not the concern of the present study.

Deleted: constitutes the most likely explanation for the large residuals observed in these regions. However, this does not constitute the topic of the current study. We therefore exclude islands and glaciers from the results and discussion. Larger dispersion values should however not prevent the discussion of the results in regions where very large residual TWS anomalies are observed, if the observed signals are several times larger than the estimated uncertainty. …

The large residuals observed with ISBA-CTRIP in the North-West of South America (Fig. 1e) are due to differences in the spatial and temporal variability of observed and predicted TWS changes. The range of TWS variations is indeed larger for ISBA-CTRIP than for GRACE in this region. R^2 values are relatively high (0.5-0.9) at the North of the Amazon, indicating important similarities between GRACE and ISBA-CTRIP. To the contrary, R^2 values are very low (< 0.3) at the South of the Amazon, indicating significant differences between GRACE and ISBA-CTRIP.

The range of TWS anomalies is smaller for hydrological models than for GRACE over most of the study area (76% for ISBA-CTRIP and 83% for WGHM). TWS anomalies predicted by hydrological models are underestimated by at least 50% over almost half of the study area (40% for ISBA-CTRIP and 49% for WGHM). TWS anomalies are at least two times smaller than GRACE for 22% of the study area for ISBA-CTRIP and 25% for WGHM. The largest range ratios (> 5) are reached across deserts (Sahara, Arabian Peninsula, Gobi Desert) and glaciers (Alaska, Patagonia, Himalaya). Such differences are due to numerical artefacts (denominator near zero) and non-hydrological signals (ice melting) observed by GRACE. Very large range ratios (2-4) are also observed for ISBA-CTRIP across the United States (Great Plains aquifer) and the North of India, because of significant anthropogenic influences in these regions, with a potential contribution of glaciers across the North of India (Blazquez et al., 2020). Large range ratios (from 2 to 5) are reached in tropical and subtropical regions of the Southern hemisphere (Africa, South-America, Australia) for WGHM.

Over more than half of the study area (61% for ISBA-CTRIP and 53% for WGHM), global hydrological models explain a minor part (R^2<0.5) of the variance of the TWS anomalies estimated with the average GRACE solution (Fig. 2c and 2d). By comparison with GRACE, WGHM is more performant in the Northern than Southern hemisphere. Relatively large R^2 values (> 0.5) are reached in the United States of America, central and North Europe, West and central Siberia, Eastern Asia, North of India, Caspian Sea and Arabian Peninsula (Fig. 2d). Large R^2 values are also reached over most of South America (Fig. 2d). Lower R^2 values (< 0.5) are reached over most of the African and Australian continents, and parts of the Northern (North Canada, central Asia, Eastern Siberia, South India) hemisphere (Fig. 2d). By comparison (Fig. 2c), ISBA-CTRIP is more performant (R^2>0.5) in the Southern hemisphere (North, Central and East Australia, South and East Africa, South-America except Peru, Bolivia and Patagonia) and parts of the Northern hemisphere (Eastern US, South Canada, central and North Europe, South of Siberia, Caspian Sea, South of India, East China). Lower R^2 values (< 0.5) are reached for ISBA-CTRIP in North Canada, West and Central Africa, Arabian Peninsula, South and central Asia and West Australia (Fig. 2c). Both models exhibit negative R^2 values in central and Sahelian Africa, as well as in Quebec and Ontario (Fig. 2c and 2d). For ISBA-CTRIP, negative R^2 coefficients are also reached in North Bolivia, Alaska, North of India and Siberia (south of Lena River). For WGHM, negative R^2 coefficients are reached in the central US and South India. These metrics indicate that for some regions of the world (not necessarily the same for both models), hydrological models are able to capture a large part of the TWS variability estimated from GRACE, but that, overall, significant differences exist between global hydrological models and GRACE satellite data.

3.2 Characteristic time scales of residual TWS anomalies

The differences in TWS anomalies estimated from GRACE and global hydrological models (or residual TWS anomalies) are largely dominated by pluri-annual and decadal signals (Fig. 3). Residual TWS anomalies have been separated into sub-annual, pluri-annual and decadal contributions using a high-pass (cut-off period at 1.5 years), band-pass (cut-off periods at 1.5 and 10 years) and low-pass (cut-off period at 10 years) filters respectively. The percentage of variance explained by each contribution has been calculated as R^2 values and reported in Maxwell's colour triangle (Fig. 3). Residual TWS anomalies are dominated by decadal signals over a large part of the study area (51% with ISBA-CTRIP and 40% with WGHM), including Alaska, West Canada, Brazilian highlands (Sao Francisco and Parana river basins), Patagonia, West (Niger and Volta river basins) and South Africa (Okavango and Zambezi river basins), parts of West (Arabic Peninsula, Caspian Sea drainage area, Tigris/Euphrates, Dnieper, Volga and Don river basins), central (Tibetan Plateau, and Tarim, Ganges and Brahmaputra river basins) and North (Yenisei and Lena river basins) Asia, and East Australia. When calculating the residuals with ISBA-CTRIP, large decadal signals are also observed across North-West America (Sierra Madre, Sierra Nevada, Great Basin, Rocky Mountains) and the North of India (Indus River basin).

Pluriannual signals are prevalent in residual TWS anomalies across central Africa, West Australia, Siberia (Ob and Yenisei), Eastern Europe, North-East America (Great Lakes) and the Southwest of the Amazon basin. Subannual signals are prevalent in regions with tenuous TWS variability (i.e., Sahara, South Africa, Southwest Australia), likely pointing out the remaining level of noise in GRACE data (Fig. 1b). Regions with large (≥ 10 cm) residual TWS anomalies (Fig. 1e), are systematically dominated by pluri-annual to decadal contributions (Fig. 3).

Residual TWS anomalies are dominated by pluri-annual and decadal changes in the TWS, including linear trends and non-linear signals (Fig. 4). Though significant linear trends are detected (+/- 1 cm/yr), residual TWS anomalies are mainly due to non-linear variability in the TWS (Fig. 4). Apart from glaciers, significant trends in TWS residuals are observed in West (Niger) and South (Okavango and Zambezi) Africa, North-East Australia, South Asia (mostly the North of India, especially when using ISBA-CTRIP), Northwest America (ISBA-CTRIP only) and central US (mainly WGHM). Part of the residual TWS trends observed with ISBA-CTRIP in Northwest America and South Asia are likely due to anthropogenic influences. In other regions of the world, residual trends in TWS are likely related to climate variability (South Africa, Northeast Australia) or land-use changes (West Africa). In most regions of the world (72% of the study area for ISBA-CTRIP and 83% for WGHM), the residual variability in TWS cannot be explained by a linear trend and involves significant variability at interannual and decadal time scales (Fig. 4c to 4f).

Deleted: slow

4 Discussion

To better characterise and understand the nature of residual TWS anomalies, TWS anomalies estimated from GRACE and global hydrological models have been averaged over large regions of the world and compared to in-situ and satellite precipitation. In the following, we discuss regional TWS anomalies where the largest residuals are observed around the central Amazon corridor, the upper Sao Francisco River, the Zambezi and Okavango rivers, the Congo River, the North of Australia, the Ogallala aquifer in central USA, the North of the Black Sea and the Northern Plains in India (see map in Fig B1 - Appendix B). For each of these regions, all the solutions of the GRACE ensemble (3 mascon and 6 spherical harmonic solutions) detect slow changes in TWS, which indicates high confidence in these observations. Larger differences occur between ISBA-CTRIP and WGHM, and both models systematically underestimate the pluri-annual and decadal changes in TWS captured by GRACE. Part of these differences may be attributed to common sources of errors in GRACE-based TWS estimates, including errors in background models (for example, the atmospheric circulation model) and post-processing choices (for example, the GIA model). However, errors in the atmospheric model (GAA from AOD1B, based on ERA5) would be associated with fast changes in TWS, while errors in the GIA model (ICE6G-D) would be characterised by linear trends over the GRACE period. Here, the largest differences between GRACE and global hydrological models occur at pluri-annual and decadal time scales, and are generally well correlated with precipitation. A large part of the differences between GRACE and global hydrological models are therefore likely to be climate-related and at least partially due to inaccurate predictions of global hydrological models. Similar regional analyses have been done for the 40 largest river basins of the world with comparable results (Appendix C).

4.1 Central Amazon Corridor

4.1.1 Study area

The central Amazon corridor (1°N-7°S and 75°W-50°W) surrounds the Solimões-Amazon mainstream river, and the downstream parts of its main tributaries, including the Japura, Jurua, Purus, Negro, Madeira, Trombetas, Tapajos and Xingu rivers. Those large rivers exhibit a monomodal flood pulse lasting several months, flooding an extensive lowland area, largely covered by forests (e.g., Junk et al., 1997; Melack and Coe, 2021). The extension of the flooded area varies from 100 000 to 600 000 km^2 in the Amazon basin (e.g., Fleishmann et al., 2022), in phase with water level variations in rivers that can reach up to 15 m annually (e.g., Birkett et al., 2002; Alsdorf et al., 2007; Frappart et al., 2012; Da Silva et al., 2012), with significant interannual variability (e.g., Fassoni-Andrade et al., 2021). Heterogeneous soils distributions, including ferralsols, plinthosols and gleysols (e.g., Quesada et al., 2011), lie over unconsolidated sedimentary rocks, alluvial deposits and consolidated sedimentary rocks with relatively homogeneous hydraulic properties (e.g., Gleeson et al., 2011; Fan et al., 2013). Across the central Amazon lowlands, the groundwater table fluctuates by several metres (Pfeffer et al., 2014), corresponding to

Formatted: Heading 2, Space Before: 0 pt, After: 0 pt, Line spacing: 1.5 lines, Don't keep with next, Border: Top: (No border), Bottom: (No border), Left: (No border), Right: (No border), Between : (No border)

Formatted: Font: Not Bold, Font colour: Auto

Deleted: , called varzea or igapo depending on the river water colour (respectively white waters rich in sediments or black waters rich in organic matter)

groundwater storage changes of several tens of centimetres (Frappart et al., 2019), which constitutes a large part of the TWS changes observed by GRACE (Frappart et al., 2019).

4.1.2 Comparison of global hydrological models with GRACE

Formatted: Heading 2, Line spacing: 1.5 lines

Over the central Amazon region (Fig. 5), TWS anomalies predicted by global hydrological models agree well with GRACE observations, with very large Pearson coefficients reached both for ISBA-CTRIP (R=0.90) and WGHM (R=0.86). The amplitudes of TWS anomalies predicted with ISBA-CTRIP match closely GRACE solutions, while WGHM tends to underestimate the TWS variability at interannual and decadal time scales, which is likely due to a more accurate representation of the floodplains and their interactions with the atmosphere, soil and aquifer with ISBA-CTRIP than WGHM (Fig. 5d). Interannual variability occurs in the precipitation as well (Fig 5a and b), with significant correlation with GRACE (R=0.54), ISBA (R=0.59) and WGHM (R=0.64) and a phase lag of 1 month. Despite good performances for both models (especially ISBA-CTRIP), significant residual signals remain in TWS anomalies after correction of hydrological effects, consisting mostly of an increasing trend with ISBA-CTRIP, with significant interannual variability superimposed for WGHM. The residual TWS changes corrected with WGHM are still significantly correlated with precipitation (R=0.48) with a phase lag of 4 months. No significant correlation can be found between the residual TWS anomalies calculated with ISBA and precipitation anomalies (maximum R value of 0.22 with a time lag of 14 months), though significant decadal and pluri-decadal variability can be observed in GPCC precipitation records, that may explain a residual trend in TWS (~ 5 mm/yr).

Residual TWS anomalies may be due to inaccurately modelled water storage variations in any reservoir from the surface to the aquifer. The largest residual TWS variations are observed along the downstream part of the Solimoes, at the confluences with the Purus and the Rio Negro, which is a region that is largely covered by floodplains (e.g., Fleishmann et al., 2022) and dominated by changes in surface water storage (Frappart et al., 2019). The long time-scales associated with the residuals and increasing time-lags with precipitation suggest however a significant contribution from groundwater storage fluctuations, that are insufficiently constrained in global hydrological models (e.g., Decharme et al., 2019, Scanlon et al., 2018 and 2019). Large floodplains may indeed delay the water transport for several months (e.g., Prigent et al., 2020), through storage and percolation from the surface towards the aquifer (e.g., Lesack & Melack, 1995; Bonnet et al., 2008; Frappart et al., 2019). Groundwater stores excess water during wet periods and sustains rivers and floodplains during low-water periods (e.g., Lesack, 1993). Groundwater systems have also been shown to convey seasonal anomalies (for example, droughts) for several years at local (e.g., Tomasella et al., 2008) and regional (Pfeffer et al., 2014) scales. Such memory effects may be underestimated by global hydrological models, which would result in much faster variations of the TWS.

4.2 Upper Sao Francisco

4.2.1 Study area

The Sao Francisco River, located in North-East Brazil, is 3200 km long and drains an area of about 630 000 km^2. Hydroelectric dams located along the Sao Francisco provide about 70% of Northeast Brazil electricity, including the Três Marias, Sobradinho and Luíz Gonzaga (Itaparica) reservoirs with respective volumes of 15,278 hm^3, 28,669 hm^3 and 3,549 hm^3. Significant decreases in the river flow during the 1980–2015 period have been attributed to increased groundwater withdrawals sustaining irrigated agriculture and decreasing the groundwater contributions to streamflow (i.e., baseflow) (Lucas et al., 2020). As a result of a prolonged drought lasting from 2002 to 2017 (Freitas et al., 2021), the Sao Francisco hydroelectric plants only provided a minor part (from 18 to 42% depending on the year) of the total electricity demand, which was sustained by increased fossil fuel consumption (de Jong et al., 2018). A decrease in TWS was also observed from 2012 to the end of the GRACE mission (mid-2017) across the Sao Francisco coincident with the observed rainfall deficit (Ndehedehe and Ferreira, 2020), allowing to better quantify the impact of prolonged droughts on the water supply in a vulnerable region (Paredes-Trejo et al., 2021).

4.2.2 Comparison of global hydrological models with GRACE

Over the upper Sao Francisco region (Fig. 6), TWS anomalies predicted with global hydrological models are well correlated with GRACE data on a year-to-year basis (R=0.79 for ISBA and R=0.81 for WGHM). The times of the minimum and maximum TWS anomalies are well picked up by satellite gravity observations and models, though the amplitude of TWS anomalies is underestimated by global hydrological models. All 9 GRACE solutions exhibit interannual and decadal variability in TWS, which is absent in both global hydrological models. In particular, GRACE monitors a drop in terrestrial water storage from 2012 to 2016 (Fig. 6b), corresponding to 4 years of consecutive deficit in precipitation (Fig. 6a), which is not picked up by global hydrological models. As a consequence, residual TWS anomalies (Fig. 6e), characterised by prominent interannual and decadal signals (Fig 6f), reach 10-20 cm in the Sao Francisco region. TWS anomalies predicted by hydrological models are relatively well correlated with precipitation (R=0.6 for ISBA and 0.52 for WGHM) with a time lag of 1 month, while the correlation with GRACE TWS anomalies is more marginal (R=0.39 with a time lag of 1 month). Residual TWS anomalies are also only marginally correlated with precipitation (R=0.29 for GRACE-WGHM and 0.33 for GRACE-ISBA), with a time lag of 3 months.

These results tend to show that global hydrological models reproduce quite well the year-to-year variability of TWS anomalies across the Sao Francisco (especially in term of occurrence of a wet/dry anomaly, as the amplitudes of the anomalies may be underestimated), but struggle to predict slower hydrological processes characterised by interannual and decadal time scales.

Formatted: Font colour: Auto

Deleted: ¶

Deleted: with

Deleted: not predicted by ISBA-CTRIP or WGHM, but

4.3 Zambezi - Okavango

4.3.1 Study area

The Zambezi River basin, located in South tropical Africa, drains an area of 1 400 000 km² connecting Angola (18.3 %), Namibia (1.2 %), Botswana (2.8 %), Zambia (40.7 %), Zimbabwe (15.9 %), Malawi (7.7 %), Tanzania (2.0 %) and Mozambique (11.4 %) (Vörösmarty and Moore III, 1991). It encompasses humid, semi-arid and arid regions dominated by seasonal rainfall patterns associated with the Inter-Tropical Convergence Zone (ITCZ), with a wet season spanning from October to April and a dry season spanning from May to September (Lowmann et al., 2018). The Zambezi basin harbours very large wetland areas and lakes, whose extension considerably varies with precipitation at seasonal and interannual time scales (Hugues et al., 2020). Significant interannual variability in the precipitation and TWS have been detected over the Zambezi and Okavango regions, and attributed to several climate modes, including the Pacific Decadal Oscillation, Atlantic Multidecadal Oscillation and El Niño Southern Oscillation (Pfeffer et al., 2021).

4.3.2 Comparison of global hydrological models with GRACE

Across the Zambezi and Okavango region (Fig. 7), TWS anomalies are well correlated with precipitation (R=0.62 and 0.49 with a time lag of 1 month for ISBA-CTRIP and WGHM). Positive (respectively negative) precipitation anomalies correspond to a local maximum (respectively minimum) in TWS. This year-to-year variability is consistent between GRACE and global hydrological models, as evidenced by a Pearson correlation coefficient of 0.60 between GRACE and ISBA-CTRIP and 0.63 between the GRACE and WGHM. However, the TWS anomalies estimated from GRACE exhibit a strong decadal oscillation with a minimum in 2005/2006 and a maximum in 2011/2012, that is not picked up by hydrological models, leaving a very strong (20 cm in amplitude) decadal anomaly in the residuals TWS. Though the residual TWS anomalies are poorly correlated with the precipitation anomaly (R=0.23 and 0.25 with a phase lag of 28 and 40 months for GRACE - ISBA and GRACE - WGHM respectively), they are strongly related to the accumulated precipitation anomalies, also exhibiting a strong decadal anomaly with a minimum in 2005/2006 and a maximum in 2011/2012.

The TWS residuals can be reduced locally by up to 50% in the Zambezi region by applying an empirical model based on climate modes, as formulated by Pfeffer et al., (2021). The main modes of variability found in the TWS residuals are the Pacific Decadal Oscillation and the Atlantic Multidecadal Oscillation.

Formatted: Border: Top: (No border), Bottom: (No border), Left: (No border), Right: (No border), Between : (No border)

Formatted: Font colour: Auto

Formatted: Font: Bold

4.4 Congo

4.4.1 Study area

The Congo basin is the second largest river basin in the world, with a drainage area of ~ 3.7 10^6 km^2 and an average annual discharge of ~ 40 500 m^3s^{-1}(Laraque et al., 2020). Despite its importance, the Congo River basin is scarcely studied (Alsdorf et al., 2016), though a growing interest arose over the past decade, substantially due to advances in satellite hydrology (e.g., Papa et al., 2022, Paris et al., 2022, Schumann et al., 2022). With an average rainfall around 1500 mm^{-1}, the Congo basin benefits from a humid tropical climate with a complex seasonal migration of rainfall across the basin with a first maximum in November-December and a second peak in April-May (Alsdorf et al., 2016) leading to a bimodal river discharge (Kitambo et al., 2022). The "Cuvette centrale" is a topographic depression located at the centre of the basin, harbouring wetlands covered by rainforests permanently or periodically flooded (Becker et al., 2018). The Congo floodplain hydrodynamics are disconnected from the main river, with much less variability observed throughout the year (Alsdorf et al., 2016). The Congo River basin hosts a large complex fractured sedimentary aquifer, with relatively low storage but high recharge rates (Scanlon et al., 2022). Very little is known about the groundwater storage variability, though comparisons of satellite estimations of the surface water storage with the total terrestrial water storage changes from GRACE, suggest that most (~ 90% at annual time scales) of the variability in water storage occurs under the surface (Becker et al., 2018).

4.4.2 Comparison of global hydrological models with GRACE

Non-seasonal TWS anomalies are very different over the Congo basin depending on the method of estimation considered (Fig. 8). All 9 GRACE solutions are consistent one with another, but differ from both global hydrological models that also exhibit large discrepancies one with another (Fig. 8). The correlations of TWS anomalies with precipitation are also marginal (maximum correlation of 0.5 with WGHM). All 9 GRACE solutions exhibit a 6-year cycle, in phase with accumulated precipitation with local minima in 2006 and 2012 and a local maxima in 2003, 2009 and 2015 (Fig. 8). Slow changes in TWS observed with GRACE are not predicted by hydrological models, leaving large residuals in TWS characterised by a ~6-year cycle (Fig. 8).

Significant power is found in multi-decadal precipitation time series at similar periods, ranging from 5 to 8 years (Laraque et al., 2020), as well as in discharge times series at 7.5 and 13.5 years (Labat et al., 2005). The variability of the TWS cannot be explained by major climate modes over the Congo River basin, except for the PDO, which may slightly influence the TWS variability at the North of the Congo River (Pfeffer et al., 2022). The variability in river discharge has been found to be temporarily consistent with NAO at 7.5 years (from the 1970s to the 1990s) and 35 years (from the 1940s to the 1990s) (Labat et al., 2005). Part of the inaccuracies in global hydrological models may be due to (i) the scarcity of in-situ data available to

Formatted: Font colour: Auto

constrain precipitation (Figure 2 in Laraque et al., 2020), (ii) errors in runoff and evapotranspiration fluxes, or (iii) unresolved underground processes, including for example preferential flow along faults (Figure 1 in Garzanti et al., 2019).

4.5 North Australia

4.5.1 Study area

The climate of Northern Australia is characterised by a wet season lasting from November to April, subject to intense thunderstorms and cyclones, with virtually no precipitation during the remainder of the year (Smith et al., 2008). Annual streamflow is highly dominated by monsoon rainfall, with dry season flows fed by groundwater discharge, that may stop for several months for a large number of rivers (Petheram et al., 2008; Smerdon et al., 2012). Groundwater plays an essential role in Northern Australia as it sustains rivers and vegetation, through baseflow and water uptake for plant transpiration (Lamontagne et al., 2005; O Grady et al., 2006). Significant interannual variability, principally related to ENSO in the North of the continent, has been observed in rainfall (Cai et al., 2011; Sharmila et al., 2020), river discharge (Chiew et al., 1998; Ward et al., 2010) and terrestrial water storage (Xie et al., 2019). During the GRACE era, Australia encountered a prolonged drought from 2002 to 2009, sometimes referred to as the 'millennium drought' or 'big dry', immediately followed by intensely wet conditions in 2010-2011 (the 'big wet' associated with La Nina) and a sustained drought, leading to another dry El Nino event in 2015 (Figure 3 in Xie et al., 2019 and Figure 9 in the present manuscript). Three major climate modes (ENSO, IOD and SAM) are necessary to explain the water storage variability across Australia, but the Northern part of the country is dominated by ENSO (Xie et al., 2019).

4.5.2 Comparison of global hydrological models with GRACE

Across North Australia (Fig. 9), TWS anomalies predicted by global hydrological models are well correlated with precipitation (R=0.73 and 0.67 with a phase lag of 1 month for ISBA and WGHM) and TWS anomalies estimated with GRACE (R=0.76 and 0.71 with ISBA and WGHM respectively). The amplitude of extreme events (for example La Niña in 2011) from ISBA matches GRACE estimates, while WGHM tends to underestimate the response of TWS to both dry (2005) and wet (2011) events (Fig. 9). The main difference between TWS estimations from global hydrological models and GRACE solutions is the pace at which TWS return to average conditions after a wet/dry event (Fig. 9). For example, after the flooding events associated with La Niña 2011, all 9 GRACE solutions estimate a slow decrease of the TWS returning to average conditions in about two years (Fig. 9). On the other hand, both global hydrological models predict a sharp decrease of the TWS returning to average conditions in about 6 months (Fig. 9). As a consequence, a positive TWS anomaly remains in the residuals after La Niña (Fig. 9), accounting for the differences in the rate of change of TWS.

Deleted: forcing such as the
Deleted: flows such as
Deleted: or
Formatted: Font colour: Auto
Formatted: Font: Bold
Deleted: annual
Deleted: event to
Deleted: velocity
Deleted: s
Deleted: in

These results are consistent with the findings of Yang et al., (2020), who found that except for the CLM-4.5 model, hydrological models underestimated the GRACE-derived TWS trends across Australia, due to inaccurately modelled contributions from soil moisture and groundwater storage. Similarly, TWS anomalies from GRACE were found to be a better link between vegetation change and climate variability than precipitation (Xie et al., 2019), because they convey more information about water availability in the soils and aquifers, especially when associated with SMOS measurements (Tian et al., 2019).

4.6 Central USA: Ogallala aquifer

4.6.1 Study area

The Ogallala, or High Plains, aquifer covers a surface area of about 450 000 km^2 across 8 states in the central USA, including parts of Colorado, Kansas, Nebraska, New Mexico, Oklahoma, South Dakota, Texas, and Wyoming. The Ogallala aquifer region supports about 20% of the wheat, corn and cotton production in the USA (Houston et al., 2013). Groundwater abstractions for irrigation began in Texas in the 1930s (Luckey et al., 1981) and exceeded recharge over much of the central and southern parts of aquifer in the 1950s (Luckey and Becker, 1999), resulting in substantial decline of the groundwater table in the Southern and Central High Plains, while the Northern High Plains stayed in balance or replenished (Haacker et al., 2016). At current depletion rates, a large part of irrigation (about 30%) may not be supported in the coming decades (Scanlon et al., 2012, Haacker et al., 2016, Steward et al., 2016, Deines et al., 2020).

4.6.2 Comparison of global hydrological models with GRACE

In the Ogallala aquifer region, all GRACE solutions exhibit a series of upwards and downwards trends in TWS with a regular increase from mid-2006 to mid-2011, a sharp decrease in TWS from mid-2011 to 2013, followed by another increase in TWS from early 2013 to 2016 (Fig. 10). This pattern is linked with precipitation anomalies that were mainly in excess over 2006-2011, in deficit over 2011/2013 and oscillated around average values over 2013-2016, with a remarkably rainy year in 2014 (Fig. 10). This succession of opposite trends is not predicted by global hydrological models (Fig. 10). WGHM does predict a sharp decrease in TWS from mid-2011 to 2013, but fails to predict the increase in TWS during 2006-2011 in spite of abundant precipitation (Fig. 10).

Such differences might be explained by an overestimation of water abstractions by WGHM, which would result in almost constant TWS changes, while precipitation, and subsequent aquifer recharge, is increasing. This assumption is supported by the work of Rateb et al. (2020), showing that global hydrological models such as WGHM or PCR-GLOBWB tend to overestimate groundwater depletion due to human intervention in the region. Good agreement is found between GRACE and in-situ observations of the groundwater table, though large uncertainties affect (i) the decomposition of the GRACE-based

Formatted: Font colour: Auto

Deleted: , though

Deleted: The TWS anomalies

Deleted: predicted by WGHM are almost constant

Deleted: during 2006-2011 are much more constant in spite of abundant precipitation.

Deleted: with

TWS anomalies into individual water reservoirs (Brookfield et al., 2018) and (ii) the estimation of hydraulic parameters (i.e. conductivity and specific yield) allowing the conversion of groundwater level variations to groundwater storage variations (Seyoum and Milewski, 2016). For the Ogallala aquifer region, GRACE data may help to characterise insufficiently well constrained parameters of WGHM, such as hydraulic parameters (i.e. conductivity, specific yield), or parameters of the water use model, such as irrigation efficiencies. In its current stage, the ISBA-CTRIP model is not adapted to estimate TWS changes in heavily managed regions, because it does not take irrigation into account.

Deleted: due to the vadose zone

Deleted: of the aquifer such as the

Deleted: or

4.7 North of India

4.7.1 Study area

Formatted: Font colour: Auto

The North of India hosts the Indus, Ganges and Brahmaputra river basins, with an average annual rainfall of 545, 1088, 2323 mm/yr respectively (e.g., Bhanja et al., 2016). The average population density ranges from 26-250 persons/km^2 in the Northwest of India to over 1000 persons/km^2 in the Northeast of India (Dangar et al., 2021). India is the largest groundwater user in the world, with an annual withdrawal of 230 -km^3 for irrigation, used essentially for rice, wheat, sugarcane, cotton and maize cultures (Mishra et al. 2018, Xie et al., 2019). High abstraction rates largely exceeding precipitation rates have been reported in Northwest India, in particular in the Punjab region, leading to an aquifer depletion rate of about 1 m/yr (Mishra et al. 2018; Dangar et al., 2021). The northern Indian plains are bordered by the Southern Tibetan plateau, whose glaciers have been undergoing significant ice thinning due to increased temperatures (e.g. Hugonnet et al., 2021). Both contributions from land hydrology and glaciers may therefore influence GRACE-based TWS estimates in this region.

4.7.2 Comparison of global hydrological models with GRACE

Formatted: Font: Bold

Because WGHM takes into account irrigation, predicted TWS anomalies match closely GRACE observations (R=0.96), leaving residuals of about +/- 2.5 cm (Fig. 11), which is about 4 to 6 times less than across the central Amazon (Fig. 5) or Zambezi (Fig. 7) regions. As expected in strongly anthropized regions, ISBA-CTRIP fails to recover the TWS changes estimated with GRACE, characterised by a clear decreasing trend (-7.71 +/- 0.71 mm/yr) over 2002-2016 (Fig. 11), clearly due to groundwater abstractions for irrigation.

Besides, the superposition of several sources of mass redistributions (i.e. land hydrology and glaciers) may generate ambiguities in the interpretation of GRACE-based TWS estimates in the North of India (Blazquez, 2020). Groundwater abstractions were however found to be the dominant driver of water mass losses across Northern India (e.g. Xiang et al., 2016). Numerous studies have reported a good agreement between in situ groundwater level measurements and GRACE TWS measurements in the North of India (e.g., Bhanja et al., 2016; Dangar et al., 2021). Detailed studies indicated that better model performances could be gained by adjustment of several parameters (water percolation rate, crop water stress, irrigation

efficiency, soil evaporation compensation and groundwater recession) against GRACE data (Xie et al., 2019). Such information is critical to ensure the reliability of hydrological models across several regions. For example, the ISBA-CTRIP model exhibit better performances than WGHM when compared to GRACE across the Indian Southern Peninsular Plateau (Figure 1), because of an overestimation of groundwater abstractions in WGHM, leading to spurious decreasing trends, not observed by satellite gravity measurements (Appendix D). An increase in TWS and replenishment of groundwater resources has indeed been reported in South India from the analysis of GRACE and wells data (e.g., Asoka et al., 2017; Bhanja et al., 2017).

4.8 North of the Black Sea

4.8.1 Study area

Formatted: Font colour: Auto

The Black Sea Catchment hosts a population of 160 million people in 23 countries drained by major rivers including the Danube, Dniester, Dnieper, Don, Kuban, Sakarya, and Kizirmak. The annual precipitation varies from less than 190 mm/yr at the Northeast of the catchment (Russia) to more than 3000 mm/yr at the West (South Austria, Slovenia, Croatia) (Rouholahnejad et al., 2014 and 2017). The annual average temperature varies from 2 to 7°C at the North of the catchment (East European Plains at the border of Ukraine, Belarus and Russia), with a local minimum (<-3°C) in the Krasnodar region (Southwest Russia) to over 15°C at the South of the Catchment (North of Turkey) (Rouholahnejad et al., 2014 and 2017). Land use in the Black Sea Catchment is dominated by agriculture (Rouholahnejad et al., 2014 and 2017).

4.8.2 Comparison of global hydrological models with GRACE

Formatted: Font: Bold

Large TWS residuals are observed in the Northeast of the Black Sea Catchment, in the East European plains crossing Ukraine, Belarus and Russia (Fig. 12). Large (~ 20 cm) TWS changes are observed by GRACE satellites in this region, characterised by a decreasing trend conjugated with significant interannual variability, with a peak at 6-7 years (Fig. 12). Such TWS changes are not predicted by hydrological models, leaving large (~15 cm) TWS residuals, dominated by decadal and interannual variability (Fig. 12).

Due to rising temperatures, a generalised drop (10-15%) in solid precipitation has been observed across the East European Plain, partially offset by liquid precipitation, except along the Northern coast of the Black and Azov Sea (drop ~ 10%), the lower Volga River Basin (drop ~ 20%) and the Dvina River Basin further North (drop ~ 25%) (Kharmalov et al., 2020). A drop in summer precipitation, together with an increase in temperature, was observed at the North of the Black, Azov and Caspian Sea, generating severe drought conditions in the region (Kharmalov et al., 2020). Water scarcity has indeed become a critical concern, with increased water stress and decreased water availability, observed today and predicted to increase in the future (Rouholahnejad et al., 2014 and 2017).

5 Conclusion

Over most (> 75%) of continental areas, non-seasonal TWS anomalies are underestimated by the global hydrological models ISBA-CTRIP and WGHM when compared to GRACE solutions. While both hydrological models agree relatively well with GRACE observations on short time scales (i.e., typically less than 2 years), they systematically underestimate slower changes in TWS observed by GRACE satellites occurring on pluri-annual to decadal time-scales. Particularly large (15 - 20 cm) residual TWS anomalies are observed across the North-East of South America (Orinoco, Amazon and Sao Francisco basins), tropical Africa (Zambezi and Congo rivers basin) and North Australia.

In such remote areas, better performances are reached with ISBA-CTRIP than WGHM, owing to the detailed representation of hydrological processes in a natural environment. However, the TWS predicted with ISBA-CTRIP still lack amplitude at pluri-annual and decadal time-scales leaving large linear (Amazon) and nonlinear (Sao Francisco, Zambezi, Congo, North Australia) trends in the TWS residuals.

The comparison of global hydrological models against GRACE data does not allow the identification of the processes responsible for these discrepancies, that could originate from any reservoir from the surface to deep aquifers. However, long time-scales associated with the residuals, combined with increasing time-lags and decreasing correlations with precipitation, suggest at least some mismodelled contributions from the groundwater cycle. Aquifers constitute the natural accumulation of runoff and precipitation, and mis-estimated parameters (hydraulic properties such as the conductivity or storage capacity) and flows (e.g., recharge, discharge, deep inflow, preferential flow along faults and fractures) may lead to significant errors in predicted groundwater storage changes. An overestimation of runoff and/or evapotranspiration may also lead to an excessively quick return of the water to the atmosphere and ocean. Evapotranspiration may in particular be difficult to estimate in regions with temporary surface water bodies (for example related to the variation of the floodplain extension, or to the formation of temporary rivers flowing during the wet season and dried up during the dry season).

If ISBA-CTRIP leads to TWS predictions in better agreement with GRACE than WGHM over remote areas, the situation is inverted for strongly anthropized regions such as the Northern Indian Plain, Central Valley (California, USA) or Great Plains (Ogallala, USA) aquifer regions. Unlike WGHM, ISBA-CTRIP does not account for human induced changes in the TWS, and is therefore not able to reproduce TWS changes in highly anthropized regions. However, important differences between GRACE and WGHM are still observed in some highly anthropized regions, such as the Ogallala aquifer, which may be due to locally mis-estimated parameters.

Large uncertainties may indeed affect the parameterisation of the water use model. For example, an overestimation of the irrigation efficiency may lead to an overestimation of evapotranspiration and underestimation of deep percolation. Errors in

such parameterisation may have a strong effect on the predicted TWS changes, that could eventually be more accurately estimated using GRACE to constrain unknown parameters. The calibration and evaluation of global hydrological models would therefore benefit the consideration of a broader range of datasets, including traditional discharge data, but also including terrestrial water storage anomalies from GRACE satellites. GRACE-based observations have for example been proven useful to quantify the impact of irrigation on groundwater resources in Northern India and improve groundwater forecasts under different Representative Concentration Pathways (RCP) in the region (Xie et al., 2020). Significant advances would be expected from the generalisation of such approaches in a dedicated framework (e.g., Condon et al., 2021, Gleeson et al., 2021).

Deleted: and GRACE-FO

Appendix A Comparison of TWS anomalies from GRACE and global hydrological models over large lakes

Residual TWS anomalies (Fig. A1) are compared for ISBA-CTRIP and WGHM with and without including the lake correction from the hydroweb database based on satellite altimetry and satellite imagery measurements. The TWS residuals are reduced for both models when applying the lake correction, especially around the Caspian Sea (- 30 cm), North American Great Lakes (-7 cm), African Great lakes (-15 cm) and Volta Lake (-5 cm). A marginal increase (+2 cm) in TWS residuals can be observed for high altitude lakes of the Tibetan plateau (e.g., Pu Moyongcuo, Yamzho Yumco, Namu Cuo, Qinghai). Slight increases in the TWS residuals (at most +1 cm) are observed in a few anthropized regions when applying the lake correction to ISBA-CTRIP, especially near the Zeya Reservoir (Russia) and the Roraima region (North Brazil). Overall, the prediction of TWS anomalies due to hydrology is improved when using the lake correction and the residual TWS anomalies are reduced.

Appendix B Location of eight regions with significant residual TWS anomalies

Residual TWS anomalies are calculated as the difference between the TWS anomalies estimated from GRACE and global hydrological models. The ensemble of residual TWS anomalies counts 18 solutions, pertaining to 9 GRACE solutions (3 mascon and 6 spherical harmonic solutions) and 2 global hydrological models (ISBA-CTRIP and WGHM). The range of average residual TWS anomalies shown in Fig. B1a depends on the systematic biases between the TWS estimates from GRACE and global hydrological models. These differences are significant if they exceed the dispersion among the 18 solutions, calculated as the difference between the 97.5 and 2.5 percentiles of the range of residual TWS anomalies (see Fig. B1b). The significance ratio of residual TWS anomalies (Fig. B1c) has been calculated to identify where the differences between GRACE solutions and hydrological models are significant, regardless of the solution or model considered. The dispersion of residual TWS solutions (Fig. B1b) is much larger than the dispersion of GRACE-based TWS solutions (Fig 1b), showing that the differences between the two models may have a large impact on the residuals and their significance.

To explore a large variety of scenarios, we selected 8 regions with large residuals (>10 cm) and high significance ratio (>2), including the central Amazon corridor (region A), the upper Sao Francisco River (region B), the Zambezi and Okavango rivers

(region C), the Congo River (region D), the North of Australia (region E), the Ogallala aquifer in central USA (region F), the North of the Black Sea (region H) and the Northern Plains in India (region G). It may be noted that the significance ratio is not extremely high across the North of India, because of the differences in the predictions of ISBA-CTRIP and WGHM. The region G was included to discuss the differences between models with respect to GRACE-based TWS anomalies. Glaciers and coastal regions have been excluded from the analyses (see section 3.1).

Appendix C Comparison of TWS anomalies from GRACE and global hydrological models over large river basins

Non-seasonal precipitation, TWS and residual TWS anomalies have been calculated and plotted for the 40 largest river basins of the world (Fig C1) according to the Global Runoff Data Centre (GRDC) Major River Basins (MRB) database (GRDC, 2020). The main conclusions drawn from global (section 3, main text) and regional (section 4, main text) analyses remain valid at basin scale. In particular, large residual TWS anomalies are observed at pluri-annual and decadal timescales, due to an underestimation of slow TWS anomalies by the two global hydrological models considered in this study (ISBA-CTRIP and WGHM) when compared to GRACE. The amplitude of ISBA-CTRIP TWS predictions is closer to GRACE in remote river basins such as the Amazon, Lake Eyre, Murray Darling, Nelson, Okavango, Orinoco, Orange and Zambezi basins. WGHM better predicts TWS anomalies observed by GRACE in anthropized basins such as the Aral Sea, Colorado, Columbia, Ganges, Indus, Rio Grande or Yellow River basins. The difference of behaviour between both hydrological models is however not systematic. For example, the TWS predictions from ISBA-CTRIP are closer to GRACE than WGHM across the Mississippi, Parana, Saint Lawrence or Yangtze basins, which are significantly affected by human interventions. Adversely, WGHM predictions fit better GRACE-based TWS anomalies than ISBA-CTRIP across the remote Yenisei and Kolyma river basins. However, it must be noted that large discrepancies are observed for both models when compared to GRACE for the Yenisei and Kolyma basins. Indeed, for a majority of basins (Dnieper, Danube, Amur, Brahmaputra, Congo, Chad, Jubba, Lena, Mackenzie, Mekong, Niger, Nile, Ob, Sao Francisco, Shatt Al Arab, Tarim He, Tocantins, Volga, Yukon), both models struggle to reproduce non-seasonal TWS anomalies at pluri-annual and decadal time-scales.

Appendix D Comparison of TWS anomalies from GRACE and global hydrological models over Southern India

TWS anomalies estimated from GRACE and global hydrological models have been averaged over Southern India and compared to in-situ and satellite precipitation (Fig. D1). The TWS anomalies captured with GRACE are well correlated with ISBA-CTRP (R=0.77) and mildly correlated (R=0.47) with WGHM predictions and precipitation (R=0.41 with a lag of 1 month). A spurious negative trend is observed in WGHM prediction over 2006-2016 (Fig. D1c), likely due to overestimated groundwater abstractions. Better performances are reached with ISBA-CTRIP, although anthropogenic contributions are neglected (Decharme et al., 2019).

Code and data availability

All code and data necessary to validate the research findings have been placed in a public repository at: https://doi.org/10.5281/zenodo.7142392

Author contribution

All authors contributed to the conceptualization of ideas presented in the manuscript. JP, AB, BD and SM provided resources necessary to conduct the research findings. JP carried out the formal analysis. AC provided research supervision and funding acquisition. All authors contributed to the investigation of research findings. JP wrote the original draft. All authors contributed to the review and editing of the manuscript.

Competing interests

The authors declare that they have no conflict of interest.

Acknowledgements

This project has received funding from the European Research Council (ERC) under the European Union's Horizon 2020 research and innovation program (GRACEFUL Synergy Grant agreement No 855677).

References

Akvas: akvas/l3py: l3py v0.1.1 (v0.1.1), Zenodo, https://doi.org/10.5281/zenodo.1450900, 2018.

Alam, S., Gebremichael, M., Ban, Z., Scanlon, B. R., Senay, G., and Lettenmaier, D. P.: Post-Drought Groundwater Storage Recovery in California's Central Valley. Water Resources Research, 57(10), e2021WR030352, 2021.

Alsdorf, D. E., Rodríguez, E., and Lettenmaier, D. P.: Measuring surface water from space, Reviews of Geophysics, 45(2), 2007.

Alsdorf, D., Beighley, E., Laraque, A., Lee, H., Tshimanga, R., O'Loughlin, F., ... and Spencer, R. G.: Opportunities for hydrologic research in the Congo Basin, Reviews of Geophysics, 54(2), 378-409, 2016.

Anyah, R. O., Forootan, E., Awange, J. L.,and Khaki, M.: Understanding linkages between global climate indices and terrestrial water storage changes over Africa using GRACE products, Science of the Total Environment, 635, 1405-1416, 2018.

Asoka, A., Gleeson, T., Wada, Y., and Mishra, V.; Relative contribution of monsoon precipitation and pumping to changes in groundwater storage in India, Nature Geoscience, 10(2), 109-117, 2017.

Becker, M., Papa, F., Frappart, F., Alsdorf, D., Calmant, S., da Silva, J. S., ... and Seyler, F; Satellite-based estimates of surface water dynamics in the Congo River Basin, International Journal of Applied Earth Observation and Geoinformation, 66, 196-209, 2018.

Bhanja, S. N., Mukherjee, A., Saha, D., Velicogna, I., and Famiglietti, J. S; Validation of GRACE based groundwater storage anomaly using in-situ groundwater level measurements in India. Journal of Hydrology, 543, 729-738, 2016.

Bhanja, S. N., Mukherjee, A., Rodell, M., Wada, Y., Chattopadhyay, S., Velicogna, I., ... and Famiglietti, J. S.; Groundwater rejuvenation in parts of India influenced by water-policy change implementation, Scientific reports, 7(1), 1-7, 2017.

Birkett, C. M., Mertes, L. A. K., Dunne, T., Costa, M. H., and Jasinski, M. J.; Surface water dynamics in the Amazon Basin: Application of satellite radar altimetry, Journal of Geophysical Research: Atmospheres, 107(D20), LBA-26, 2002.

Blazquez, A., Meyssignac, B., Bertier E., Longuevergne L., and Creteaux J.-F.; Combining space gravimetry observations with data from satellite altimetry and high resolution visible imagery to resolve mass changes of endorheic basins and exorheic basins, in preparation for Geophysical Research Letters, 2022.

Bonnet, M. P., et al.; Floodplain hydrology in an Amazon floodplain lake (Lago Grande de Curuaí), J. Hydrol., 349(1), 18–30, 2008.

Brookfield, A. E., Hill, M. C., Rodell, M., Loomis, B. D., Stotler, R. L., Porter, M. E., and Bohling, G. C.; In situ and GRACE-based groundwater observations: Similarities, discrepancies, and evaluation in the High Plains aquifer in Kansas, Water Resources Research, 54(10), 8034-8044, 2018.

Cáceres, D., Marzeion, B., Malles, J. H., Gutknecht, B. D., Müller Schmied, H., and Döll, P.; Assessing global water mass transfers from continents to oceans over the period 1948–2016, Hydrology and Earth System Sciences, 24(10), 4831-4851, 2020.

Cai, W., Whetton, P. H., and Pittock, A. B; Fluctuations of the relationship between ENSO and northeast Australian rainfall, Climate Dynamics, 17(5), 421-432, 2001.

Chandanpurkar, H. A., Reager, J. T., Famiglietti, J. S., and Syed, T. H.; Satellite-and reanalysis-based mass balance estimates of global continental discharge (1993–2015), Journal of Climate, 30(21), 8481-8495, 2017.

Chen, J., Famiglietti, J. S., Scanlon, B. R., and Rodell, M.; Groundwater storage changes: present status from GRACE observations, In Remote Sensing and Water Resources (pp. 207-227), Springer, Cham, 2016.

Chen, J., Cazenave, A., Dahle, C., Llovel, W., Panet, I., Pfeffer, J., and Moreira, L.; Applications and challenges of GRACE and GRACE follow-on satellite gravimetry, Surveys in Geophysics, 1-41, 2022.

Chiew, F. H., Piechota, T. C., Dracup, J. A., and McMahon, T. A.; El Nino/Southern Oscillation and Australian rainfall, streamflow and drought: Links and potential for forecasting, Journal of hydrology, 204(1-4), 138-149, 1998.

Condon, L.E., Kollet, S., Bierkens, M.F., Fogg, G.E., Maxwell, R.M., Hill, M.C., Fransen, H.J.H., Verhoef, A., Van Loon, A.F., Sulis, M. and Abesser, C.; Global groundwater modeling and monitoring: Opportunities and challenges, Water Resources Research, 57(12), p.e2020WR029500, 2021.

Crétaux, J. F., Abarca-del-Río, R., Berge-Nguyen, M., Arsen, A., Drolon, V., Clos, G., and Maisongrande, P.; Lake volume monitoring from space, Surveys in Geophysics, 37(2), 269-305, 2016.

Dahle, C., Flechtner, F., Murböck, M., Michalak, G., Neumayer, H., Abrykosov, O., Reinhold, A. and König, R.; GRACE Geopotential GSM Coefficients GFZ RL06, V. 6.0, GFZ Data Services, https://doi.org/10.5880/GFZ.GRACE_06_GSM, 2018.

Dangar, S., Asoka, A., and Mishra, V.; Causes and implications of groundwater depletion in India: A review, Journal of Hydrology, 596, 126103, 2021.

Da Silva, J. S., Seyler, F., Calmant, S., Rotunno Filho, O. C., Roux, E., Araújo, A. A. M., and Guyot, J. L, Water level dynamics of Amazon wetlands at the watershed scale by satellite altimetry, International Journal of Remote Sensing, 33(11), 3323-3353, 2012.

Decharme, B., Delire, C., Minvielle, M., Colin, J., Vergnes, J. P., Alias, A., ... and Voldoire, A.; Recent changes in the ISBA-CTRIP land surface system for use in the CNRM-CM6 climate model and in global off-line hydrological applications, Journal of Advances in Modeling Earth Systems, 11(5), 1207-1252, 2019.

Dee, D. P., Uppala, S. M., Simmons, A. J., Berrisford, P., Poli, P., Kobayashi, S., ... and Vitart, F.; The ERA-Interim reanalysis: Configuration and performance of the data assimilation system, Quarterly Journal of the royal meteorological society, 137(656), 553-597, 2011.

De Jong, P., Tanajura, C. A. S., Sánchez, A. S., Dargaville, R., Kiperstok, A., and Torres, E. A; Hydroelectric production from Brazil's São Francisco River could cease due to climate change and inter-annual variability, Science of the Total Environment, 634, 1540-1553, 2018.

Deines, J. M., Schipanski, M. E., Golden, B., Zipper, S. C., Nozari, S., Rottler, C., ... and Sharda, V.; Transitions from irrigated to dryland agriculture in the Ogallala Aquifer: Land use suitability and regional economic impacts, Agricultural Water Management, 233, 106061, 2020.

Ditmar, P.; Conversion of time-varying Stokes coefficients into mass anomalies at the Earth's surface considering the Earth's oblateness, Journal of Geodesy, 92(12), 1401-1412, 2018.

Dobslaw, H., Bergmann-Wolf, I., Dill, R., Poropat, L., Thomas, M., Dahle, C., ... and Flechtner, F.; A new high-resolution model of non-tidal atmosphere and ocean mass variability for de-aliasing of satellite gravity observations: AOD1B RL06, Geophysical Journal International, 211(1), 263-269, 2017.

Döll, P., Fritsche, M., Eicker, A., and Müller Schmied, H.; Seasonal water storage variations as impacted by water abstractions: comparing the output of a global hydrological model with GRACE and GPS observations, Surveys in Geophysics, 35(6), 1311-1331, 2014a.

Döll, P., Müller Schmied, H., Schuh, C., Portmann, F. T., and Eicker, A.; Global-scale assessment of groundwater depletion and related groundwater abstractions: Combining hydrological modeling with information from well observations and GRACE satellites, Water Resources Research, 50(7), 5698-5720, 2014b.

Fan, Y., H. Li, and G. Miguez-Macho; Global patterns of groundwater table depth, Science, 339(6122), 940– 943, 2013.

Fassoni-Andrade, A. C., Fleischmann, A. S., Papa, F., Paiva, R. C. D. D., Wongchuig, S., Melack, J. M., ... and Pellet, V.; Amazon hydrology from space: scientific advances and future challenges, Reviews of Geophysics, 59(4), e2020RG000728, 2021.

Felfelani, F., Wada, Y., Longuevergne, L., and Pokhrel, Y. N.; Natural and human-induced terrestrial water storage change: A global analysis using hydrological models and GRACE, Journal of Hydrology, 553, 105-118, 2017.

Fleischmann, A. S., Papa, F., Fassoni-Andrade, A., Melack, J. M., Wongchuig, S., Paiva, R. C. D., ... and Collischonn, W.; How much inundation occurs in the Amazon River basin?, Remote Sensing of Environment, 278, 113099, 2022.

Frappart, F., Papa, F., da Silva, J. S., Ramillien, G., Prigent, C., Seyler, F., and Calmant, S.; Surface freshwater storage and dynamics in the Amazon basin during the 2005 exceptional drought, Environmental Research Letters, 7(4), 044010, 2012.

Frappart, F., and Ramillien, G.; Monitoring groundwater storage changes using the Gravity Recovery and Climate Experiment (GRACE) satellite mission: A review, Remote Sensing, 10(6), 829, 2018.

Frappart, F., Papa, F., Güntner, A., Tomasella, J., Pfeffer, J., Ramillien, G., ... and Seyler, F.; The spatio-temporal variability of groundwater storage in the Amazon River Basin, Advances in Water Resources, 124, 41-52, 2019.

Freitas, A. A., Drumond, A., Carvalho, V. S., Reboita, M. S., Silva, B. C., and Uvo, C. B.; Drought assessment in São Francisco river basin, Brazil: characterization through SPI and associated anomalous climate patterns, Atmosphere, 13(1), 41, 2021.

Garzanti, E., Vermeesch, P., Vezzoli, G., Andò, S., Botti, E., Limonta, M., ... and Yaya, N. K.; Congo River sand and the equatorial quartz factory, Earth-Science Reviews, 197, 102918, 2019.

Gleeson, T., L. Smith, N. Moosdorf, J. Hartmann, H. H. Dürr, A. H. Manning, L. P. H. van Beek, and A. M. Jellinek; Mapping permeability over the surface of the Earth, Geophys. Res. Lett., 38, L02401, doi:10.1029/2010GL045565, 2011.

Gleeson, T., Wagener, T., Döll, P., Zipper, S. C., West, C., Wada, Y., Taylor, R., Scanlon, B., Rosolem, R., Rahman, S., Oshinlaja, N., Maxwell, R., Lo, M.-H., Kim, H., Hill, M., Hartmann, A., Fogg, G., Famiglietti, J. S., Ducharne, A., de Graaf, I., Cuthbert, M., Condon, L., Bresciani, E., and Bierkens, M. F. P.; GMD perspective: The quest to improve the evaluation of groundwater representation in continental- to global-scale models, Geosci. Model Dev., 14, 7545–7571, https://doi.org/10.5194/gmd-14-7545-202, 2021.

Goux O., Pfeffer J., Blazquez A., Weaver A. T., and Ablain M.; Mass conserving filter based on diffusion for Gravity Recovery and Climate Experiment (GRACE) spherical harmonics solutions, in revision for Geophys. J. Int, 2022.

GRACE-FO; GRACEFO_L2_JPL_MONTHLY_0060. Ver. 6. PO.DAAC, CA, USA, Dataset accessed 2022-01-05 at https://doi.org/10.5067/GFL20-MJ060, 2019a.

GRACE-FO; GRACEFO_L2_CSR_MONTHLY_0060. Ver. 6. PO.DAAC, CA, USA, Dataset accessed 2022-01-05 at https://doi.org/10.5067/GFL20-MC060, 2019b.

GRDC; Major River Basins of the World / Global Runoff Data Centre, GRDC. 2nd, rev. ext. ed. Koblenz, Germany: Federal Institute of Hydrology (BfG), 2020.

Haacker, E. M., Kendall, A. D., and Hyndman, D. W.; Water level declines in the High Plains Aquifer: Predevelopment to resource senescence, Groundwater, 54(2), 231-242, 2016.

Herbert, C. and Döll, P.; Global assessment of current and future groundwater stress with a focus on transboundary aquifers, Water Resources Research, 55, 4760– 4784, https://doi.org/10.1029/2018WR023321, 2019.

Houston, N. A., Gonzales-Bradford, S. L., Flynn, A. T., Qi, S. L., Peterson, S. M., Stanton, J. S., ... and Senay, G. B.; Geodatabase Compilation of Hydrogeologic, Remote Sensing, and Water-Budget-Component Data for the High Plains Aquifer, 2011, US Geological Survey Data Series, 777, 12, 2013.

Huffman, G.J., E.F. Stocker, D.T. Bolvin, E.J. Nelkin and J. Tan; GPM IMERG Final Precipitation L3 1 month 0.1 degree x 0.1 degree V06, Greenbelt, MD, Goddard Earth Sciences Data and Information Services Center (GES DISC), Accessed: 26 January 2022, 10.5067/GPM/IMERG/3B-MONTH/06, 2019.

Hughes, D. A., Mantel, S., and Farinosi, F.; Assessing development and climate variability impacts on water resources in the Zambezi River basin: Initial model calibration, uncertainty issues and performance, Journal of Hydrology: Regional Studies, 32, 100765, 2020.

Humphrey, V., Gudmundsson, L., and Seneviratne, S. I., Assessing global water storage variability from GRACE: Trends, seasonal cycle, subseasonal anomalies and extremes, Surveys in Geophysics, 37(2), 357-395, 2016.

Junk, W. J.; The Central Amazon floodplain: Ecology of a pulsing system, Ecological Studies. Berlin, Germany: Springer, 1997.

Kharlamov, M., and Kireeva, M.; Drought dynamics in the East European Plain for the period 1980-2018, In E3S Web of Conferences (Vol. 163, p. 02004), EDP Sciences, 2020.

Kitambo, B., Papa, F., Paris, A., Tshimanga, R. M., Calmant, S., Fleischmann, A. S., ... and Andriambeloson, J.; A combined use of in situ and satellite-derived observations to characterize surface hydrology and its variability in the Congo River Basin, Hydrology and Earth System Sciences, 26(7), 1857-1882, 2022.

Labat, D., Ronchail, J., and Guyot, J. L.; Recent advances in wavelet analyses: Part 2—Amazon, Parana, Orinoco and Congo discharges time scale variability, Journal of Hydrology, 314(1-4), 289-311, 2005.

Lamontagne, S., Cook, P. G., O'Grady, A., and Eamus, D.; Groundwater use by vegetation in a tropical savanna riparian zone (Daly River, Australia), Journal of Hydrology, 310(1-4), 280-293, 2005.

Landerer, F. W., Flechtner, F. M., Save, H., Webb, F. H., Bandikova, T., Bertiger, W. I., ... and Yuan, D. N.; Extending the global mass change data record: GRACE Follow-On instrument and science data performance, Geophysical Research Letters, 47(12), e2020GL088306, 2020.

Laraque, A., Moukandi N'kaya, G. D., Orange, D., Tshimanga, R., Tshitenge, J. M., Mahé, G., ... and Gulemvuga, G.; Recent budget of hydroclimatology and hydrosedimentology of the congo river in central Africa, Water, 12(9), 2613, 2020.

Lemoine, J. M., and Bourgogne, S.; RL05 monthly and 10-day gravity field solutions from CNES/GRGS (No. GSTM2020-51), Copernicus Meetings, 2020.

Lesack, L. F.; Water balance and hydrologic characteristics of a rain forest catchment in the central Amazon basin, Water Resour. Res., 29(3), 759– 773, 1993.

Lesack, L. F., and J. M. Melack; Flooding hydrology and mixture dynamics of lake water derived from multiple sources in an Amazon floodplain lake, Water Resour. Res., 31(2), 329– 345, 1995.

Loomis, B.D., Luthcke, S.B. and Sabaka, T.J.; Regularization and error characterization of GRACE mascons. J Geod **93,** 1381–1398. https://doi.org/10.1007/s00190-019-01252-y, 2019a.

Loomis, B. D., Rachlin, K. E., and Luthcke, S. B.; Improved Earth oblateness rate reveals increased ice sheet losses and mass-driven sea level rise, Geophysical Research Letters, 46(12), 6910-6917, 2019b.

Lowman, L. E., Wei, T. M., and Barros, A. P.; Rainfall variability, wetland persistence, and water–carbon cycle coupling in the Upper Zambezi river basin in Southern Africa, Remote Sensing, 10(5), 692, 2018.

Lucas, M. C., Kublik, N., Rodrigues, D. B., Meira Neto, A. A., Almagro, A., Melo, D. D. C., ... and Oliveira, P. T. S., Significant baseflow reduction in the sao francisco river basin, Water, 13(1), 2, 2020.

Luckey, R., and M. Becker; Hydrogeology, water use, and simulation of flow in the High Plains Aquifer in north-western Oklahoma, southeastern Colorado, southwester Kansas, northeastern New Mexico, and northwestern Texas, Water-Resources Investigations Report 99-4104, Reston,Virginia: USGS, 1999.

Luckey, R.R., E.D. Gutentag, and J.B. Weeks.; Water-level and saturated thickness changes, predevelopment to 1980, in the High Plains Aquifer in parts of Colorado, Kansas, Nebraska, New Mexico, Oklahoma, South Dakota, Texas, and Wyoming, Hydrologic Investigations Atlas HA-652, Reston, Virginia: USGS, 1981.

Marzeion, B., Jarosch, A. H., and Hofer, M.; Past and future sea-level change from the surface mass balance of glaciers, The Cryosphere, 6(6), 1295-1322, 2012.

Mayer-Gürr, T., Behzadpour, S., Ellmer, M., Kvas, A., Klinger, B., Strasser, S. and Zehentner, N.; ITSG-Grace2018 - Monthly, Daily and Static Gravity Field Solutions from GRACE, GFZ Data Services, https://doi.org/10.5880/ICGEM.2018.003, 2018.

Melack, J. M., and Coe, M. T; Amazon floodplain hydrology and implications for aquatic conservation, Aquatic Conservation: Marine and Freshwater Ecosystems, 31(5), 1029-1040, 2021.

Meyer, U., Lasser, M., Jaeggi, A., Dahle, C., Flechtner, F., Kvas, A., Behzadpour, S., Mayer-Gürr, T., Lemoine, J., Koch, I., Flury, J., Bourgogne, S.; International Combination Service for Time-variable Gravity Fields (COST-G) Monthly GRACE-FO Series, V. 01, GFZ Data Services, https://doi.org/10.5880/ICGEM.COST-G.002, , 2020.

Mishra, V., Asoka, A., Vatta, K., and Lall, U.; Groundwater depletion and associated CO2 emissions in India, Earth's Future, 6(12), 1672-1681, 2018.

Müller Schmied, H., Cáceres, D., Eisner, S., Flörke, M., Herbert, C., Niemann, C., Peiris, T. A., Popat, E., Portmann, F. T., Reinecke, R., Schumacher, M., Shadkam, S., Telteu, C.-E., Trautmann, T., and Döll, P.; The global water resources and use model WaterGAP v2.2d: model description and evaluation, Geosci. Model Dev., 14, 1037–1079, https://doi.org/10.5194/gmd-14-1037-2021, 2021.

Ndehedehe, C. E., and Ferreira, V. G; Assessing land water storage dynamics over South America, Journal of Hydrology, 580, 124339, 2020.

Ni, S., Chen, J., Wilson, C. R., Li, J., Hu, X., and Fu, R.; Global terrestrial water storage changes and connections to ENSO events, Surveys in Geophysics, 39(1), 1-22, 2018.

NOAA National Geophysical Data Center; ETOPO1 1 Arc-Minute Global Relief Model, NOAA National Centers for Environmental Information, Accessed 14th December 2020, 2009.

O'Grady, A. P., Eamus, D., Cook, P. G., and Lamontagne, S.; Groundwater use by riparian vegetation in the wet–dry tropics of northern Australia, Australian Journal of Botany, 54(2), 145-154, 2006.

Ojha, C., Shirzaei, M., Werth, S., Argus, D. F., and Farr, T. G.; Sustained groundwater loss in California's Central Valley exacerbated by intense drought periods, Water Resources Research, 54(7), 4449-4460, 2018.

Papa, F., Crétaux, J. F., Grippa, M., Robert, E., Trigg, M., Tshimanga, R. M., ... and Calmant, S.; Water resources in Africa under global change: monitoring surface waters from space, Surveys in Geophysics, 1-51, 2022.

Paredes-Trejo, F., Barbosa, H. A., Giovannettone, J., Kumar, T. L., Thakur, M. K., Buriti, C. D. O., and Uzcátegui-Briceño, C.; Drought assessment in the São Francisco River Basin using satellite-based and ground-based indices, Remote Sensing, 13(19), 3921, 2021.

Paris, A., Calmant, S., Gosset, M., Fleischmann, A. S., Conchy, T. S. X., Garambois, P. A., ... and Laraque, A.; Monitoring Hydrological Variables from Remote Sensing and Modeling in the Congo River Basin, Congo Basin Hydrology, Climate, and Biogeochemistry: A Foundation for the Future, 339-366, 2022.

Peltier, W. R., D. F. Argus, and R. Drummond; Comment on the paper by Purcell et al. 2016 entitled An assessment of ICE-6G_C (VM5a) glacial isostatic adjustment model, J. Geophys. Res. Solid Earth, 122, 2018.

Petheram, C., McMahon, T. A., and Peel, M. C.; Flow characteristics of rivers in northern Australia: implications for development. Journal of Hydrology, 357(1-2), 93-111, 2008.

Pfeffer, J., Seyler, F., Bonnet, M.-P., Calmant, S., Frappart, F., Papa, F., Paiva, R. C. D., Satgé, F., and Silva, J. S. D.; Low-water maps of the groundwater table in the central Amazon by satellite altimetry, Geophys. Res. Lett., 41, 1981–1987, doi:10.1002/2013GL059134, 2014.

Pfeffer, J., Cazenave, A., and Barnoud, A.; Analysis of the interannual variability in satellite gravity solutions: detection of climate modes fingerprints in water mass displacements across continents and oceans, Climate Dynamics, 58(3), 1065-1084, 2022.

Prigent, C., Jimenez, C., and Bousquet, P.; Satellite-derived global surface water extent and dynamics over the last 25 years (GIEMS-2), Journal of Geophysical Research: Atmospheres, 125(3), e2019JD030711, 2020.

Quesada, C. A., Lloyd, J., Anderson, L. O., Fyllas, N. M., Schwarz, M., and Czimczik, C. I.; Soils of Amazonia with particular reference to the RAINFOR sites, Biogeosciences, 8(6), 1415-1440, 2011.

RGI Consortium, Randolph Glacier Inventory - A Dataset of Global Glacier Outlines, Version 6. Boulder, Colorado USA. NSIDC: National Snow and Ice Data Center. doi: **https://doi.org/10.7265/4m1f-gd79**, 2017.

Rateb, A., Scanlon, B. R., Pool, D. R., Sun, A., Zhang, Z., Chen, J., ... and Zell, W.; Comparison of groundwater storage changes from GRACE satellites with monitoring and modeling of major US aquifers, Water Resources Research, 56(12), e2020WR027556, 2020.

Rodell, M., Chen, J., Kato, H., Famiglietti, J. S., Nigro, J., and Wilson, C. R.; Estimating groundwater storage changes in the Mississippi River basin (USA) using GRACE, Hydrogeology Journal, 15(1), 159-166, 2007.

Rodell, M., Famiglietti, J. S., Wiese, D. N., Reager, J. T., Beaudoing, H. K., Landerer, F. W., and Lo, M. H.; Emerging trends in global freshwater availability, Nature, 557(7707), 651-659, 2018.

Rouholahnejad, E., Abbaspour, K. C., Srinivasan, R., Bacu, V., & Lehmann, A. (2014). Water resources of the Black Sea Basin at high spatial and temporal resolution. Water Resources Research, 50(7), 5866-5885.

Rouholahnejad, E., Abbaspour, K. C., and Lehmann, A.; Water resources of the Black Sea catchment under future climate and land use change projections, Water, 9(8), 598, 2017.

Save, H., S. Bettadpur, and B.D. Tapley; High resolution CSR GRACE RL05 mascons, J. Geophys. Res. Solid Earth, 121, doi:10.1002/2016JB013007, 2016.

Save, H.; CSR GRACE and GRACE-FO RL06 Mascon Solutions v02, doi: 10.15781/cgq9-nh24, 2020.

Scanlon, B. R., Longuevergne, L., and Long, D.; Ground referencing GRACE satellite estimates of groundwater storage changes in the California Central Valley, USA, Water Resources Research, 48(4), 2012.

Scanlon, B. R., Faunt, C. C., Longuevergne, L., Reedy, R. C., Alley, W. M., McGuire, V. L., and McMahon, P. B.; Groundwater depletion and sustainability of irrigation in the US High Plains and Central Valley, Proceedings of the national academy of sciences, 109(24), 9320-9325, 2012.

Scanlon, B. R., Zhang, Z., Save, H., Sun, A. Y., Müller Schmied, H., Van Beek, L. P., ... and Bierkens, M. F.; Global models underestimate large decadal declining and rising water storage trends relative to GRACE satellite data, Proceedings of the National Academy of Sciences, 115(6), E1080-E1089, 2018.

Scanlon, B. R., Zhang, Z., Rateb, A., Sun, A., Wiese, D., Save, H., ... and Reedy, R. C.; Tracking seasonal fluctuations in land water storage using global models and GRACE satellites, Geophysical Research Letters, 46(10), 5254-5264, 2019.

Scanlon, B. R., Rateb, A., Anyamba, A., Kebede, S., MacDonald, A. M., Shamsudduha, M., ... and Xie, H.; Linkages between GRACE water storage, hydrologic extremes, and climate teleconnections in major African aquifers, Environmental Research Letters, 17(1), 014046, 2022.

Schneider, U., Becker, A., Finger, P. et al.; GPCC's new land surface precipitation climatology based on quality-controlled in situ data and its role in quantifying the global water cycle, Theor Appl Climatol **115,** 15–40; https://doi.org/10.1007/s00704-013-0860-x; 2014.

Schumann, G. J. P., Moller, D. K., Croneborg-Jones, L., and Andreadis, K. M.; Reviewing Applications of Remote Sensing Techniques to Hydrologic Research in Sub-Saharan Africa, with a Special Focus on the Congo Basin, Congo Basin Hydrology, Climate, and Biogeochemistry: A Foundation for the Future, 295-321, 2022.

Seyoum, W. M., and Milewski, A. M.; Monitoring and comparison of terrestrial water storage changes in the northern high plains using GRACE and in-situ based integrated hydrologic model estimates, Advances in Water Resources, 94, 31-44, 2016.

Sharmila, S., and Hendon, H. H.; Mechanisms of multiyear variations of Northern Australia wet-season rainfall. Scientific reports, 10(1), 1-11, 2020.

Smith, I. N., Wilson, L., and Suppiah, R.; Characteristics of the northern Australian rainy season. Journal of Climate, 21(17), 4298-4311, 2008.

Smerdon, B. D., Gardner, W. P., Harrington, G. A., and Tickell, S. J.; Identifying the contribution of regional groundwater to the baseflow of a tropical river (Daly River, Australia), Journal of Hydrology, 464, 107-115, 2012.

Steward, D. R., and Allen, A. J.; Peak groundwater depletion in the High Plains Aquifer, projections from 1930 to 2110, Agricultural Water Management, 170, 36-48, 2016.

Sun, Y., Riva, R., and Ditmar, P.; Optimizing estimates of annual variations and trends in geocenter motion and J2 from a combination of GRACE data and geophysical models, Journal of Geophysical Research: Solid Earth, 121(11), 8352-8370, 2016.

Sun, Z., Zhu, X., Pan, Y., and Zhang, J.; Assessing terrestrial water storage and flood potential using GRACE data in the Yangtze River basin, China. Remote Sensing, 9(10), 1011, 2017.

Syed, T. H., Famiglietti, J. S., and Chambers, D. P.; GRACE-based estimates of terrestrial freshwater discharge from basin to continental scales, Journal of Hydrometeorology, 10(1), 22-40, 2009.

Syed, T. H., Famiglietti, J. S., Chambers, D. P., Willis, J. K., and Hilburn, K.; Satellite-based global-ocean mass balance estimates of interannual variability and emerging trends in continental freshwater discharge, Proceedings of the National Academy of Sciences, 107(42), 17916-17921, 2010.

Tang, L., Li, J., Chen, J., Wang, S. Y., Wang, R., and Hu, X.; Seismic impact of large earthquakes on estimating global mean ocean mass change from GRACE, Remote Sensing, 12(6), 935, 2020.

Tapley, B. D., Bettadpur, S., Ries, J. C., Thompson, P. F., and Watkins, M. M.; GRACE measurements of mass variability in the Earth system, Science, 305(5683), 503-505, 2004.

Thomas, B. F., Famiglietti, J. S., Landerer, F. W., Wiese, D. N., Molotch, N. P., and Argus, D. F.; GRACE groundwater drought index: Evaluation of California Central Valley groundwater drought, Remote Sensing of Environment, 198, 384-392, 2017.

Thomas, B. F., and Famiglietti, J. S.; Identifying climate-induced groundwater depletion in GRACE observations, Scientific reports, 9(1), 1-9, 2019.

Tian, S., Renzullo, L. J., Van Dijk, A. I., Tregoning, P., and Walker, J. P.; Global joint assimilation of GRACE and SMOS for improved estimation of root-zone soil moisture and vegetation response, Hydrology and Earth System Sciences, 23(2), 1067-1081, 2019.

Tomasella, J., M. G. Hodnett, L. A. Cuartas, A. D. Nobre, M. J. Waterloo, and S. M. Oliveira; The water balance of an Amazonian micro-catchment: The effect of interannual variability of rainfall on hydrological behaviour, Hydrol. Process., 22(13), 2133– 2147, 2008.

Voldoire, A., Saint-Martin, D., Sénési, S., Decharme, B., Alias, A., Chevallier, M., et al.; Evaluation of CMIP6 DECK experiments with CNRM-CM6-1, Journal of Advances in Modeling Earth Systems, 11, 2177– 2213, https://doi.org/10.1029/2019MS001683, 2019.

Vörösmarty, C. J., and Moore, B.; Modeling basin-scale hydrology in support of physical climate and global biogeochemical studies: An example using the Zambezi River, Surveys in Geophysics, 12(1), 271-311, 1991.

Wada, Y., Wisser, D., and Bierkens, M. F.; Global modeling of withdrawal, allocation and consumptive use of surface water and groundwater resources, Earth System Dynamics, 5(1), 15-40, 2014.

Wahr, J., Molenaar, M., and Bryan, F.; Time variability of the Earth's gravity field: Hydrological and oceanic effects and their possible detection using GRACE, Journal of Geophysical Research: Solid Earth, 103(B12), 30205-30229, 1998.

Ward, P. J., Beets, W., Bouwer, L. M., Aerts, J. C., and Renssen, H.; Sensitivity of river discharge to ENSO, Geophysical Research Letters, 37(12), 2010.

Weedon, G. P., Balsamo, G., Bellouin, N., Gomes, S., Best, M. J., and Viterbo, P.; The WFDEI meteorological forcing data set: WATCH Forcing Data methodology applied to ERA-Interim reanalysis data, Water Resources Research, 50(9), 7505-7514, 2014.

Wiese, D. N. , D.-N. Yuan, C. Boening, F. W. Landerer, and M. M. Watkins; JPL GRACE and GRACE-FO Mascon Ocean, Ice, and Hydrology Equivalent Water Height JPL RL06 Version 02. Ver. 2. PO.DAAC, CA, USA, Dataset accessed 2022-01-05 at https://doi.org/10.5067/TEMSC-3MJ62, 2019.

Xie, Z., Huete, A., Cleverly, J., Phinn, S., McDonald-Madden, E., Cao, Y., and Qin, F.; Multi-climate mode interactions drive hydrological and vegetation responses to hydroclimatic extremes in Australia, Remote sensing of Environment, 231, 111270, 2019.

Xie, H., Longuevergne, L., Ringler, C., and Scanlon, B. R.; Integrating groundwater irrigation into hydrological simulation of India: Case of improving model representation of anthropogenic water use impact using GRACE, Journal of Hydrology: Regional Studies, 29, 100681, 2020.

Yang, X., Tian, S., Feng, W., Ran, J., You, W., Jiang, Z., and Gong, X.; Spatio-temporal evaluation of water storage trends from hydrological models over Australia using GRACE mascon solutions, Remote Sensing, 12(21), 3578, 2020.

Yuan D.-N.; GRACE Follow-On Level-2 Gravity Field Product User Handbook, JPL D-103922, https://podaac-tools.jpl.nasa.gov/drive/files/allData/gracefo/docs/GRACE-FO_L2-UserHandbook_v1.0.pdf, 2019.

Zhuang J., Dussin R., Jüling A. and Rasp S.; JiaweiZhuang/xESMF: v0.3.0 Adding ESMF.LocStream capabilities (v0.3.0). Zenodo. https://doi.org/10.5281/zenodo.3700105, 2020.

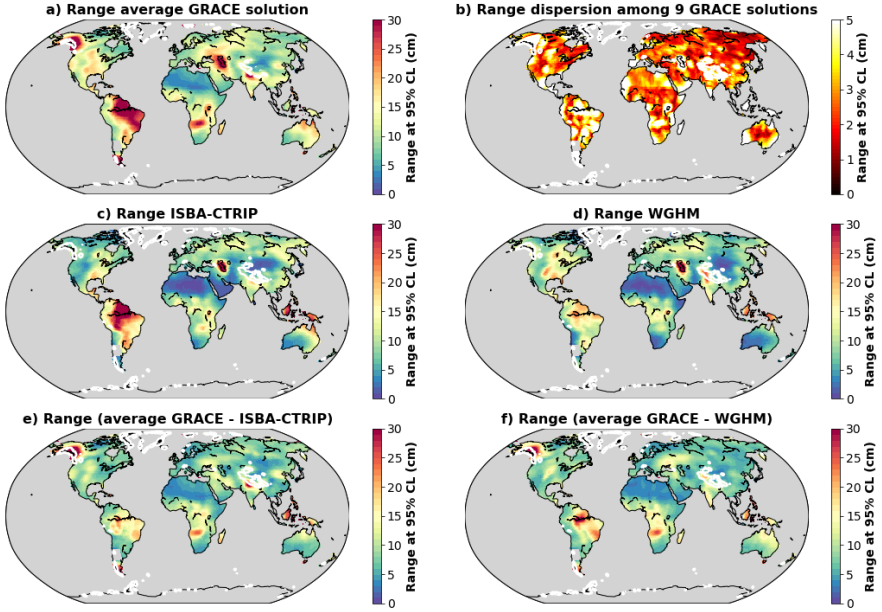

Figure 1: Comparison of TWS anomalies estimated from an ensemble of nine GRACE solutions and two global hydrological models. The amplitude of the non-seasonal TWS variability is expressed as the range at 95% CL, calculated as the difference between the 97.5 and 2.5 percentiles of the TWS anomalies obtained in each grid cell over the entire study period. TWS predictions from global hydrological models should not be compared with GRACE data around glaciers, identified by white contours. a) Range of TWS anomalies estimated as the average of nine GRACE solutions. b) Dispersion of the range of TWS anomalies among nine GRACE solutions. Range of TWS anomalies estimated with ISBA-CTRIP (c) and WGHM (d). Range of residual TWS anomalies estimated as the difference between the average of 9 GRACE solutions and ISBA-CTRIP (e) or WGHM (f).

Formatted: Font colour: Auto

Formatted: Font: Not Bold, Font colour: Auto

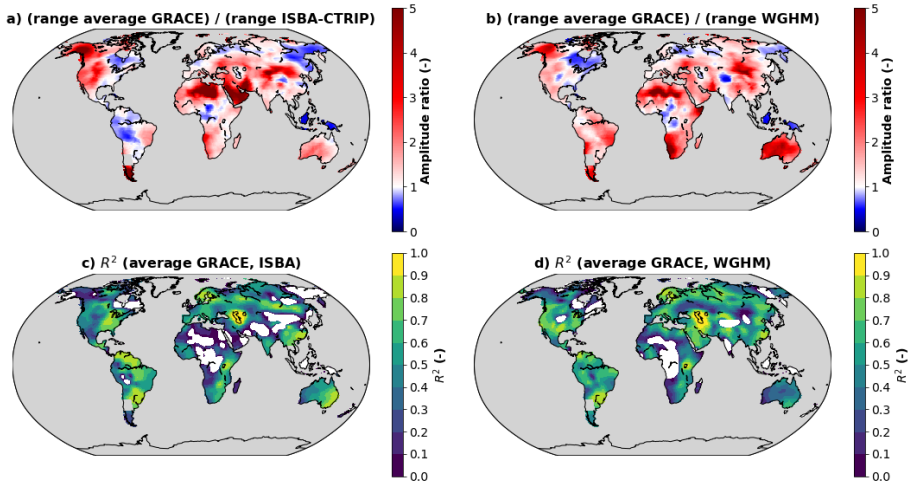

63

64 **Figure 2: Range ratios between the average GRACE solution and the hydrological models ISBA-CTRIP (a) and**
65 **WGHM (b). Determination coefficients between the average GRACE solution and the hydrological models ISBA-**
66 **CTRIP (c) and WGHM (d). Regions, where the coefficient of determination is negative, are shown in white**

67

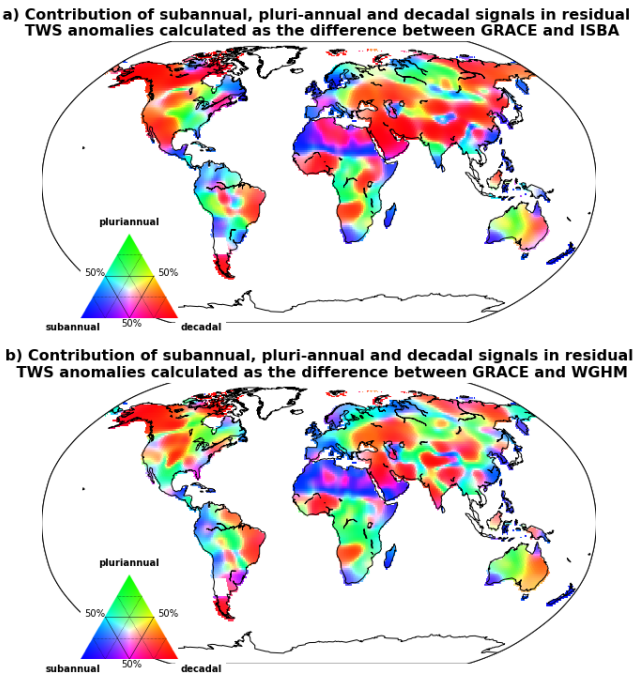

Figure 3: Characteristic time scales in residual TWS anomalies calculated as the differences between the average GRACE solution and ISBA-CTRIP (a) or WGHM (b). Subannual, pluriannual and decadal contributions have been computed with high-pass (cut-off period at 1.5 years), band-pass (cut-off periods at 1.5 and 10 years) and low-pass (cut-off period at 10 years) filters respectively. The percentage of variance explained by one contribution has been calculated as the coefficient of determination with respect to the full residual signal.

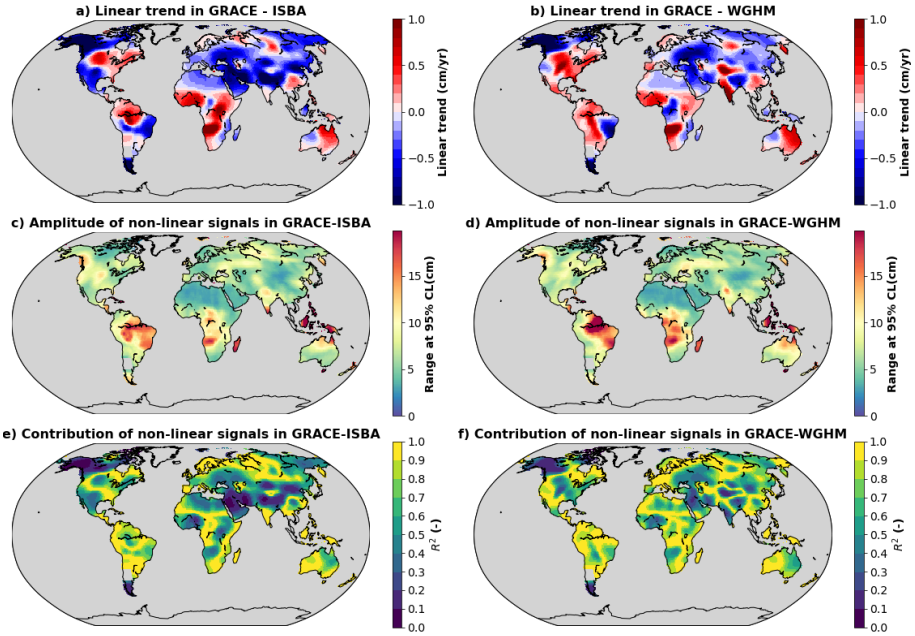

Figure 4: a) Linear trends in residual TWS anomalies calculated as the difference between the average GRACE solution and ISBA-CTRIP. b) Same as (a) with WGHM. c) Amplitude of non-linear signals in residual TWS anomalies calculated as the difference between the average GRACE solution and ISBA-CTRIP. The amplitude is calculated as the difference between the 97.5 and 2.5 percentiles. d) Same as (c) with WGHM. e) Coefficient of determination calculated for non-linear signals with respect to TWS anomalies calculated as the difference between the average GRACE solution and ISBA-CTRIP. f) Same as (e) with WGHM.

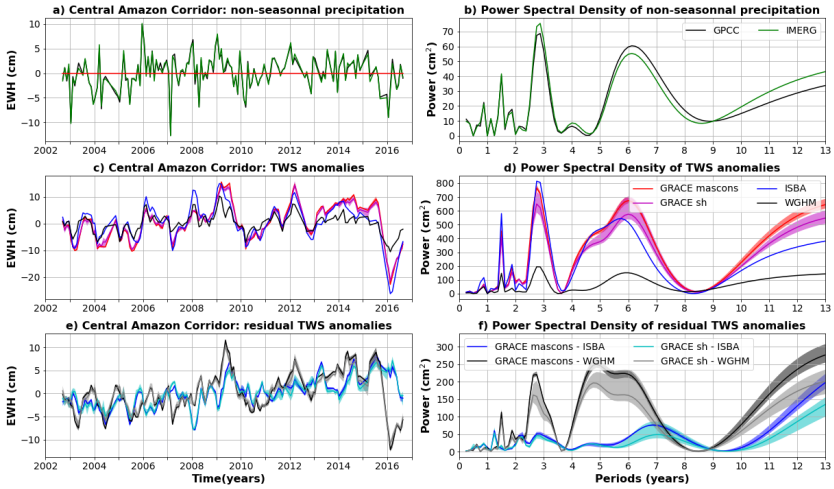

Figure 5: Comparison of TWS and precipitation anomalies averaged over the Central Amazon Corridor (box A in Fig. B1 - Appendix B). a) Average precipitation anomalies for the GPCC (gauge-based) and IMERG (satellite-based) products. b) Power Spectral Density (PSD) of average precipitation anomalies. c) TWS anomalies average over the central Amazon for two global hydrological models (ISBA-CTRIP in blue and WGHM in black) and 9 GRACE solutions (mascons in red, spherical harmonic in magenta). The solid line corresponds to the average of the sub-ensemble, the shaded area to the minimum to maximum envelope. d) PSD of the averaged TWS anomalies shown in (c). e) Residual TWS anomalies averaged over the central Amazon corridor and calculated as the difference between GRACE and ISBA-CTRIP (blue when the difference is calculated with mascons, cyan with spherical harmonics) or WGHM (black when the difference is calculated with mascons, grey with spherical harmonics).

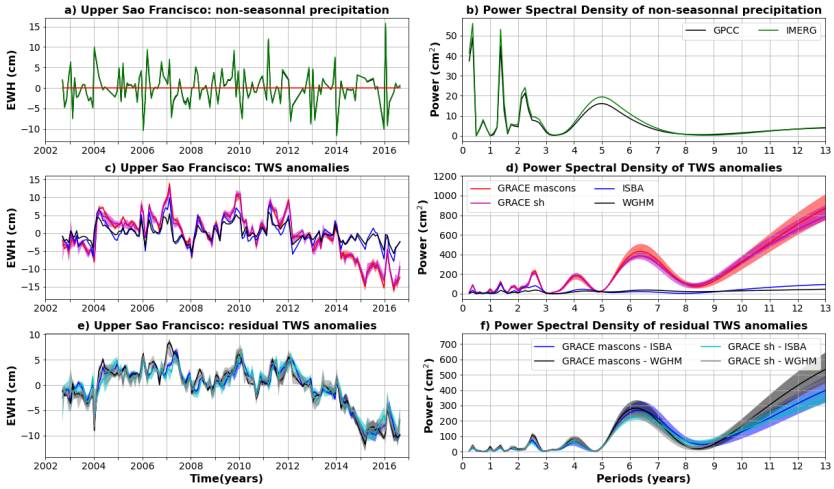

94

95 **Figure 6: Same as Fig. 5 but for the Upper Sao Francisco (box B in Fig. B1 - Appendix B).**

96

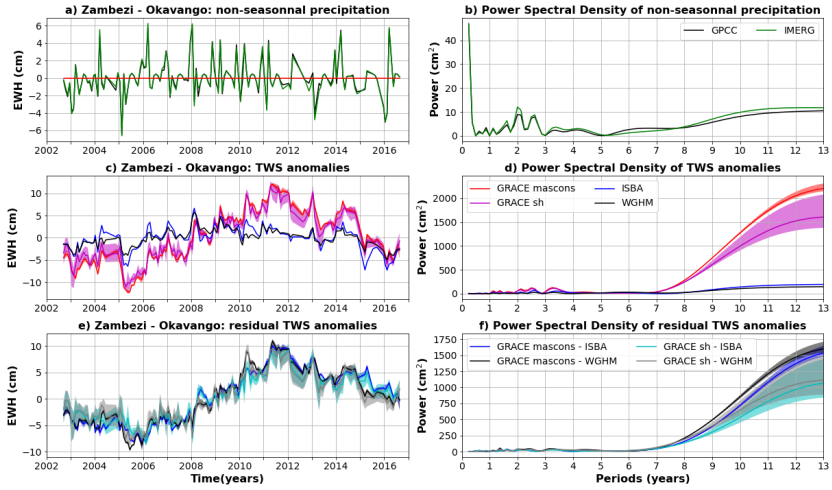

97

98 **Figure 7: Same as Fig. 5 but for the Zambezi and Okavango rivers (box C in Fig. B1 - Appendix B).**

99

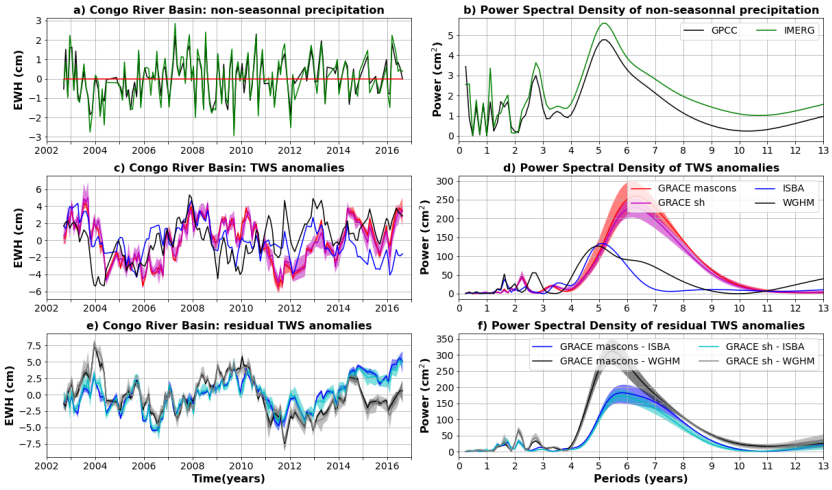

00

01 **Figure 8: Same as Fig. 5 but for the Congo River (box D in Fig. B1 - Appendix B).**

02

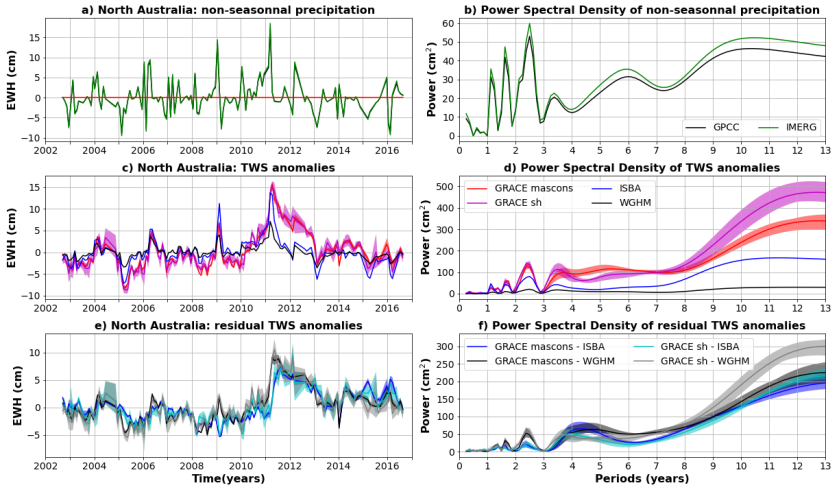

03

04 **Figure 9: Same as Fig. 5 but for North Australia (box E in Fig. B1 - Appendix B).**

05

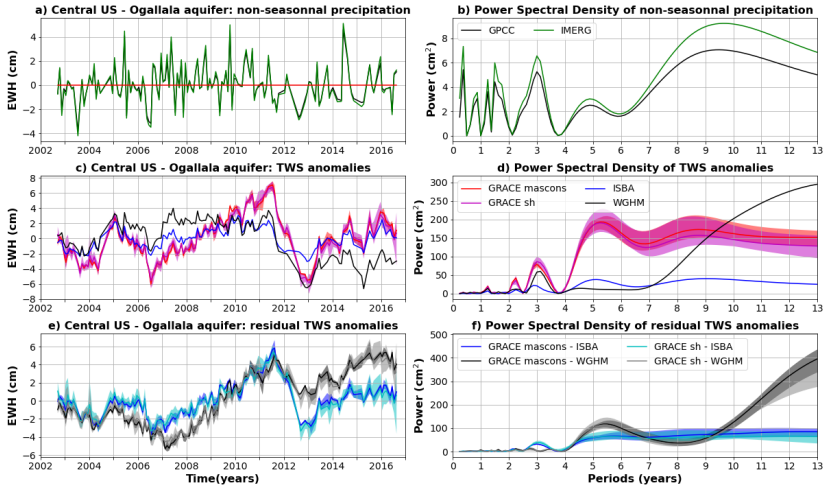

06

07 **Figure 10: Same as Fig. 5 but for the Central USA - Ogallala aquifer region (box F in Fig. B1 - Appendix B).**

08

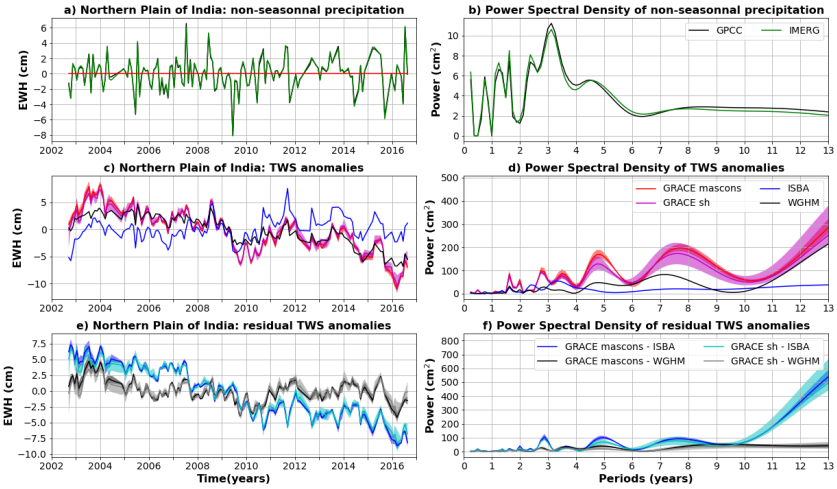

09

10 **Figure 11: Same as Fig. 5 but for the Indian Northern Plains (box G in Fig. B1 - Appendix B).**

11

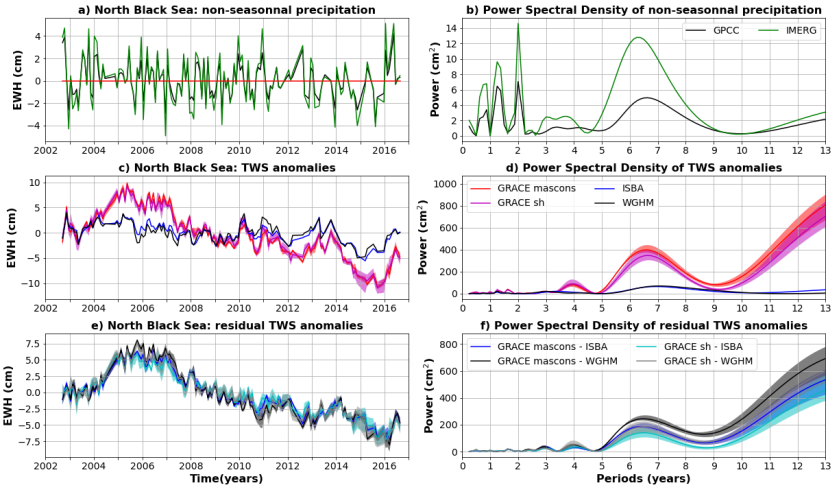

Figure 12: Same as Fig. 5 but for the North of the Black Sea (box H in Fig. B1 - Appendix B).

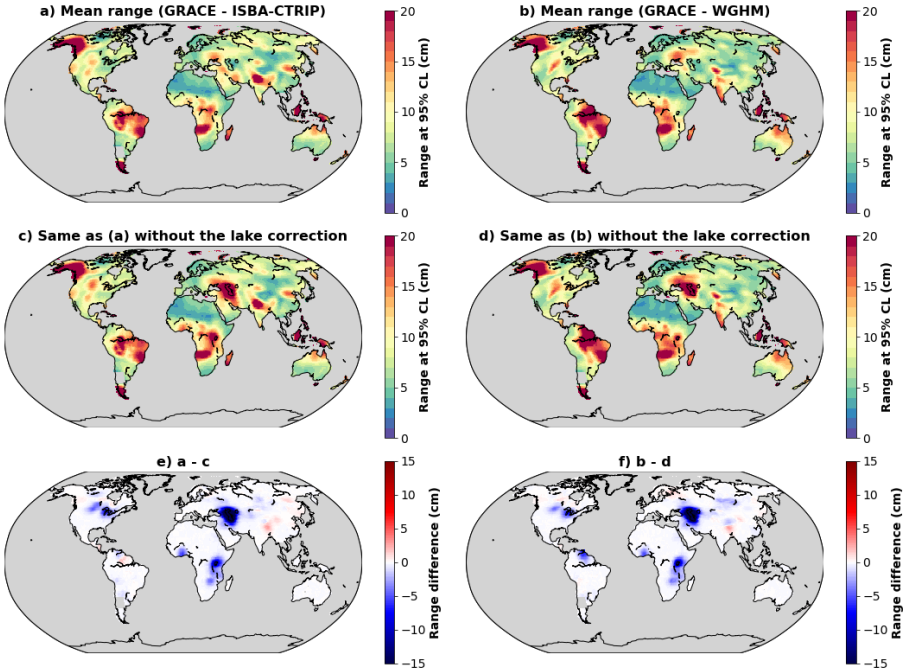

Figure A1: a) Range of residual TWS anomalies calculated with ISBA-CTRIP. b) Range of residual TWS anomalies calculated with WGHM. c) Range of residual TWS anomalies calculated with ISBA-CTRIP without including the lake correction. d) Range of residual TWS anomalies calculated with WGHM without including the lake correction. d) Difference between a and c due to the lake correction. e) Difference between b and d due to the lake correction.

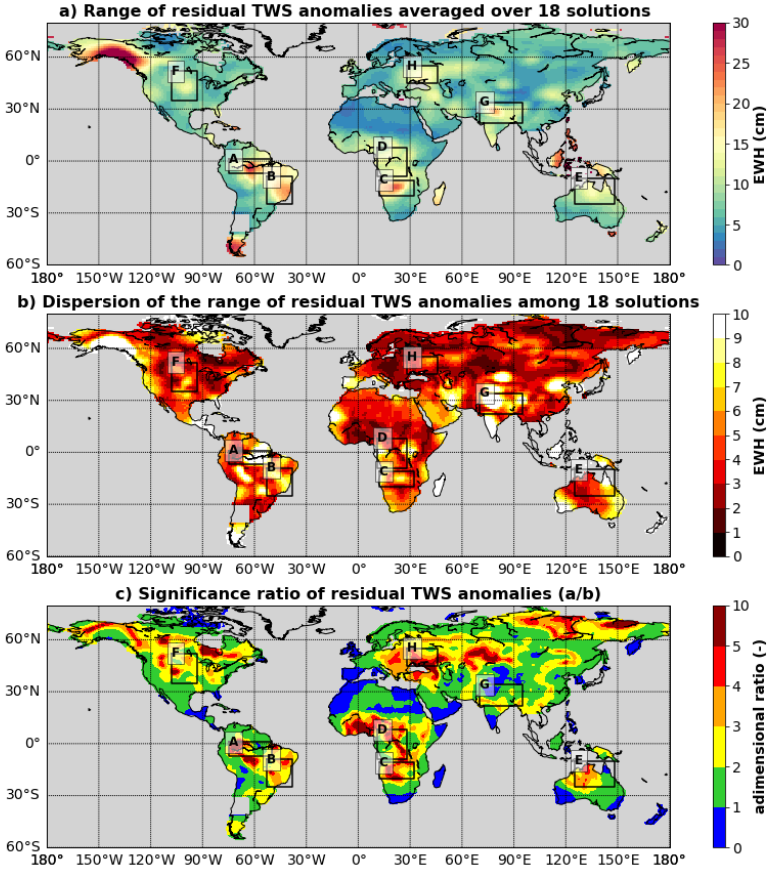

Figure B1: a) Average range of 18 residual TWS anomalies. b) Dispersion of the range of residual TWS anomalies. The dispersion is calculated as the difference between the 97.5 and 2.5 percentiles of the range of 18 residual TWS anomalies. c) Significance ratio of the averaged residual TWS anomalies calculated as the average range of residual TWS anomalies (a) divided by the dispersion of the range among the 18 solutions (b).

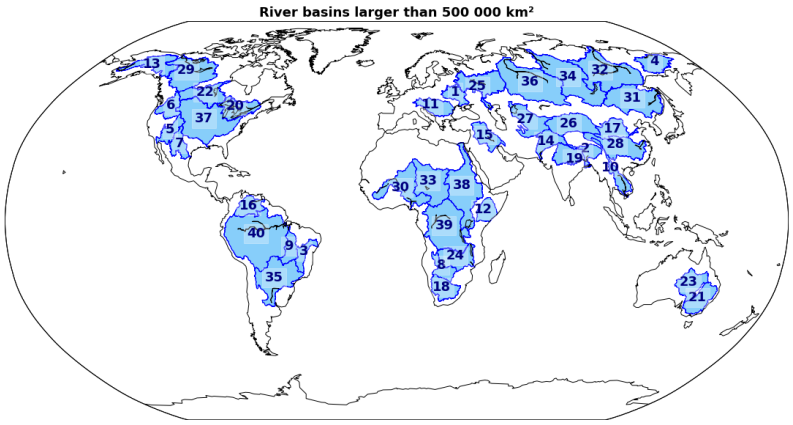

Figure C1: Map of the 40 largest river basins considered in this study: 1) Dnieper, 2) Brahmaputra, 3) Sao Francisco, 4) Kolyma, 5) Colorado, 6) Columbia, 7) Rio Grande, 8) Okavango, 9) Tocantins, 10) Mekong, 11) Danube, 12) Jubba, 13) Yukon, 14) Indus, 15) Shatt Al Arab, 16) Orinoco, 17) Yellow River, 18) Orange, 19) Ganges, 20) Saint Lawrence, 21) Murray, 22) Nelson, 23) Lake Eyre, 24) Zambezi, 25) Volga, 26) Tarim He, 27) Aral Sea, 28) Yangtze, 29) Mackenzie, 30) Niger, 31) Amur, 32) Lena, 33) Chad, 34) Yenisei, 35) Parana, 36) Ob, 37) Mississippi, 38) Nile, 39) Congo, 40) Amazon.

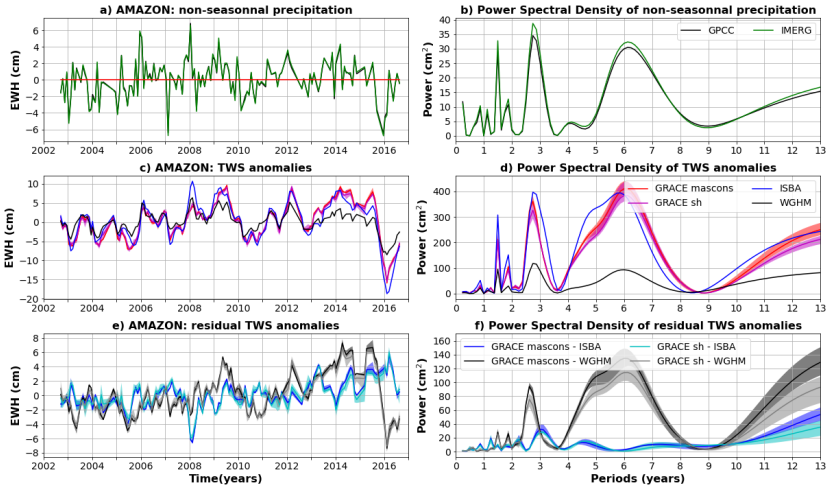

Figure C2: Comparison of TWS and precipitation anomalies averaged over Amazon basin. a) Average precipitation anomalies for the GPCC (gauge-based) and IMERG (satellite-based) products. b) Power Spectral Density (PSD) of average precipitation anomalies. c) TWS anomalies average over the central Amazon for two global hydrological models (ISBA-CTRIP in blue and WGHM in black) and 9 GRACE solutions (mascons in red, spherical harmonic in magenta). The solid line corresponds to the average of the sub-ensemble, the shaded area to the minimum to maximum envelope. d) PSD of the averaged TWS anomalies shown in (c). e) Residual TWS anomalies averaged over the central Amazon corridor and calculated as the difference between GRACE and ISBA-CTRIP (blue when the difference is calculated with mascons, cyan with spherical harmonics) or WGHM (black when the difference is calculated with mascons, grey with spherical harmonics).

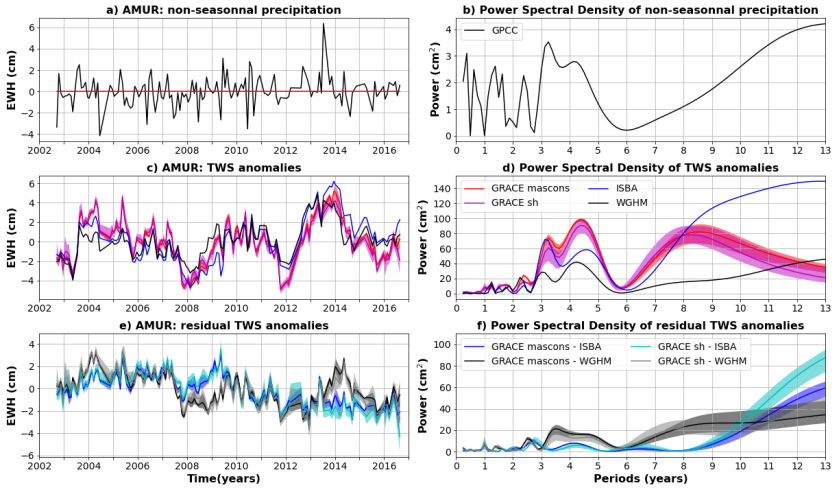

Figure C3: Same as C2 for the Amur Basin. Non-seasonal precipitation anomalies are only estimated with GPCC, as a significant part of the basin is not covered by IMERG satellites due to the high latitude of the Amur basin.

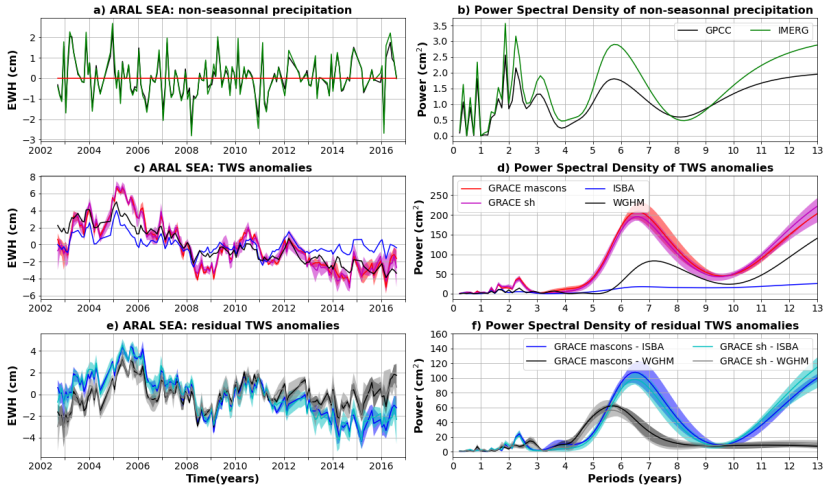

Figure C4: Same as C2 for the Aral Sea basin.

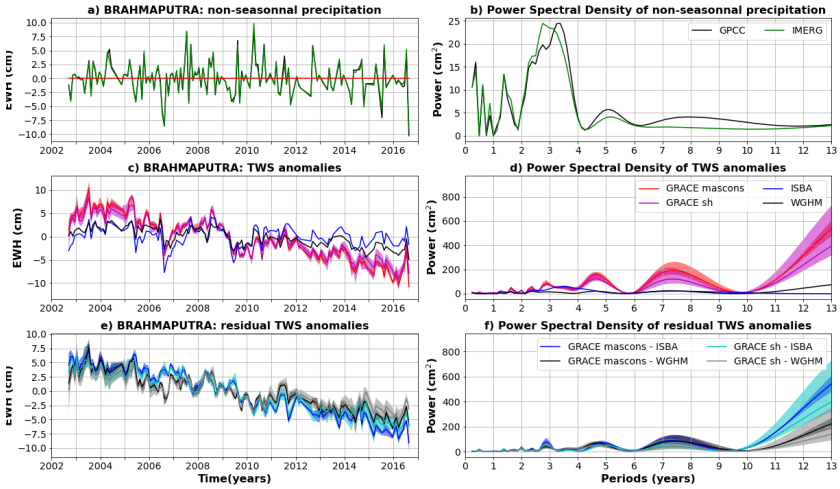

56

57 **Figure C5: Same as C2 for the Brahmaputra basin.**

58

59

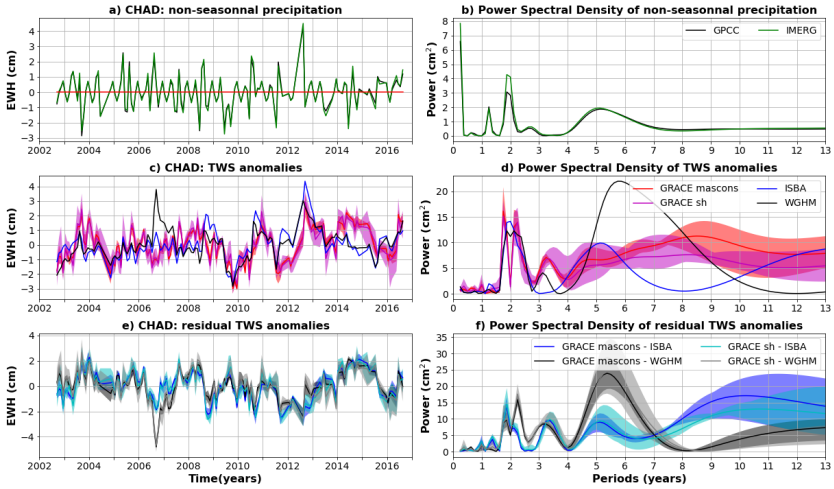

Figure C6: Same as C2 for the Chad basin.

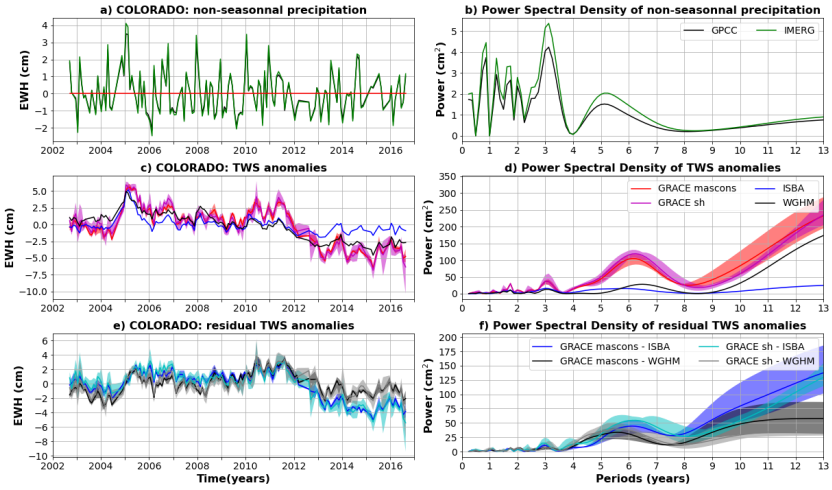

63

64 **Figure C7: Same as C2 for the Colorado basin.**

65

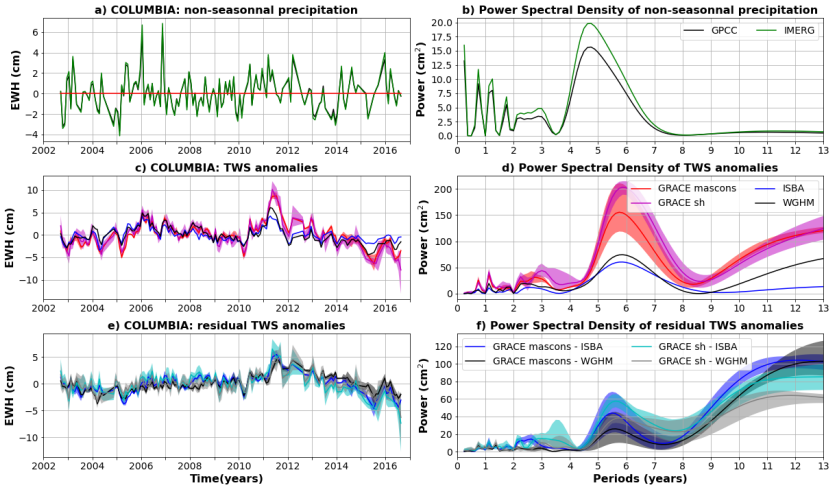

Figure C8: Same as C2 for the Columbia basin.

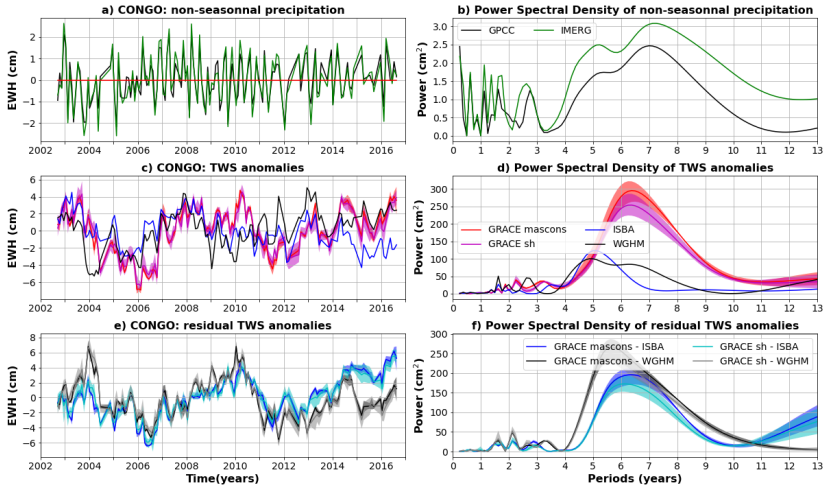

Figure C9: Same as C2 for the Congo basin.

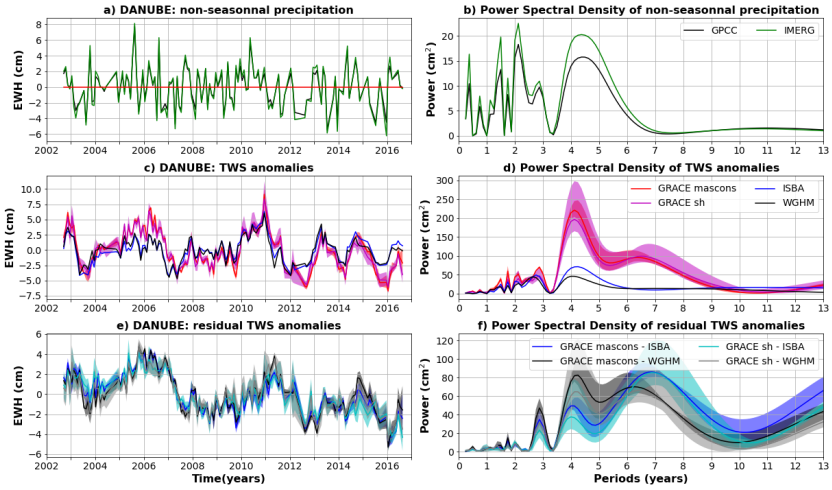

72

73 **Figure C10: Same as C2 for the Danube basin.**

74

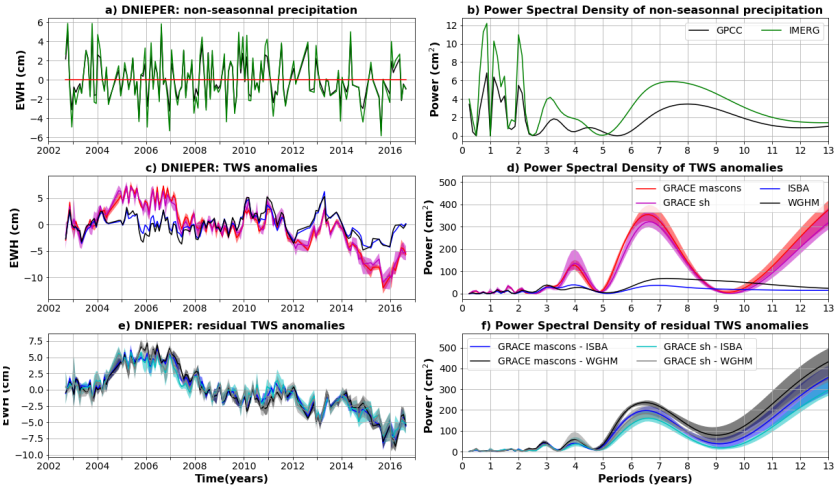

Figure C11: Same as C2 for the Dnieper basin.

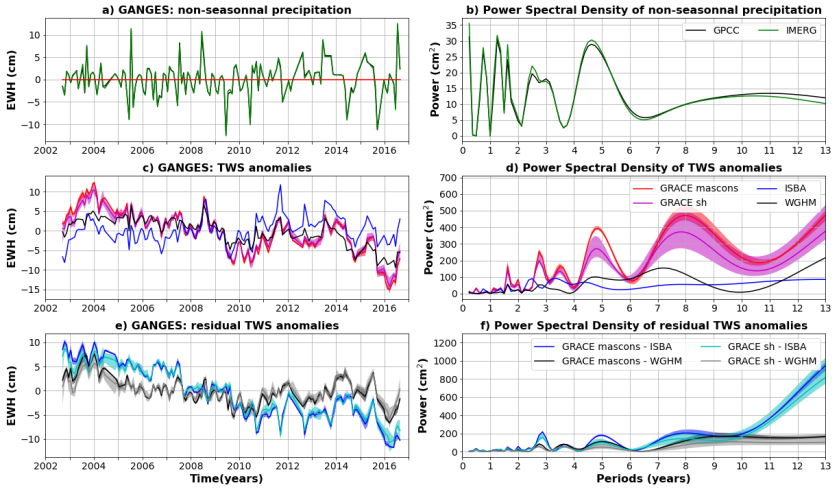

79

80 **Figure C12: Same as C2 for the Ganges basin.**

81

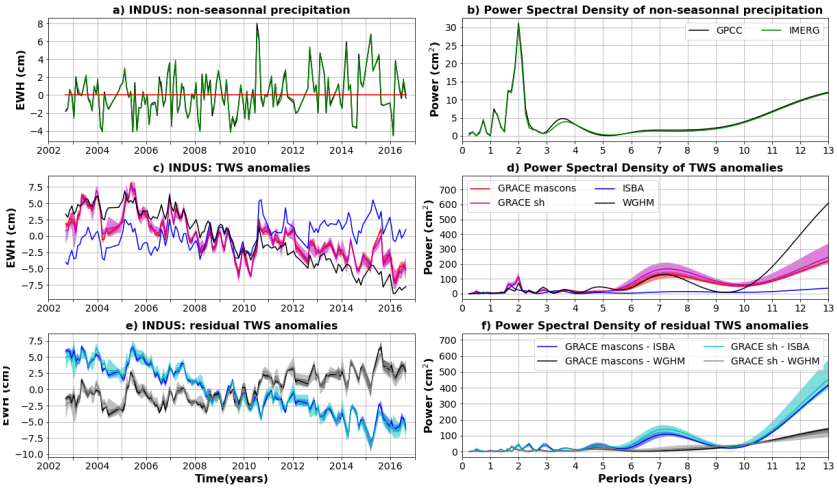

Figure C13: Same as C2 for the Indus basin.

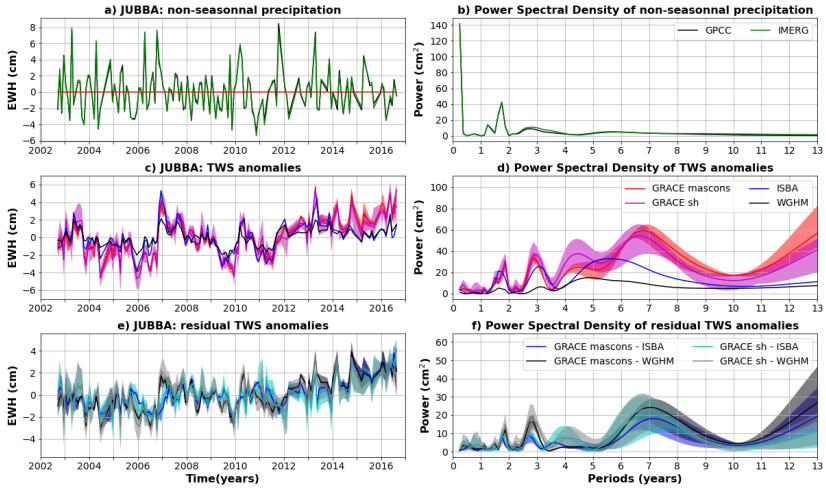

86

87 **Figure C14: Same as C2 for the Jubba basin.**

88

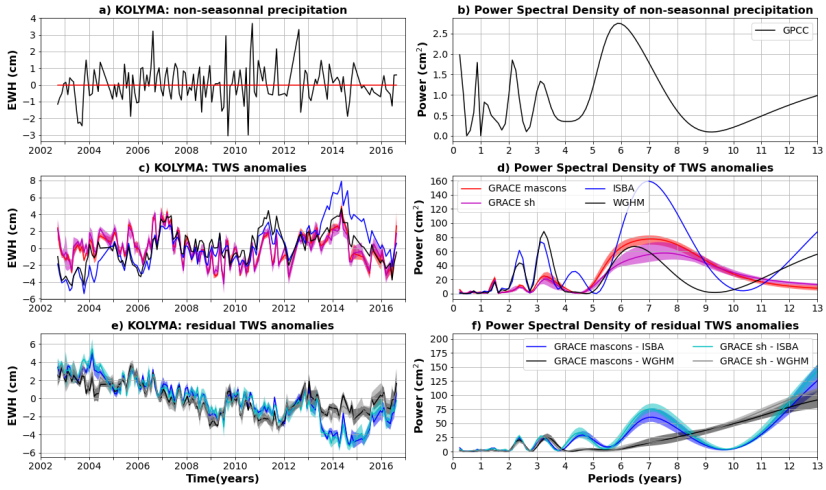

Figure C15: Same as C2 for the Kolyma basin. Non-seasonal precipitation anomalies are only estimated with GPCC, as a significant part of the river basin is not covered by IMERG satellites due to its high latitude.

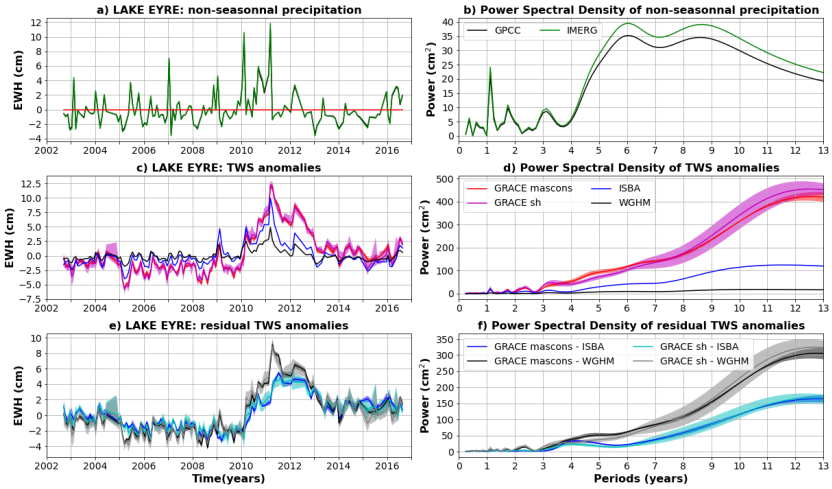

93

94 **Figure C16: Same as C2 for the Lake Eyre basin.**

95

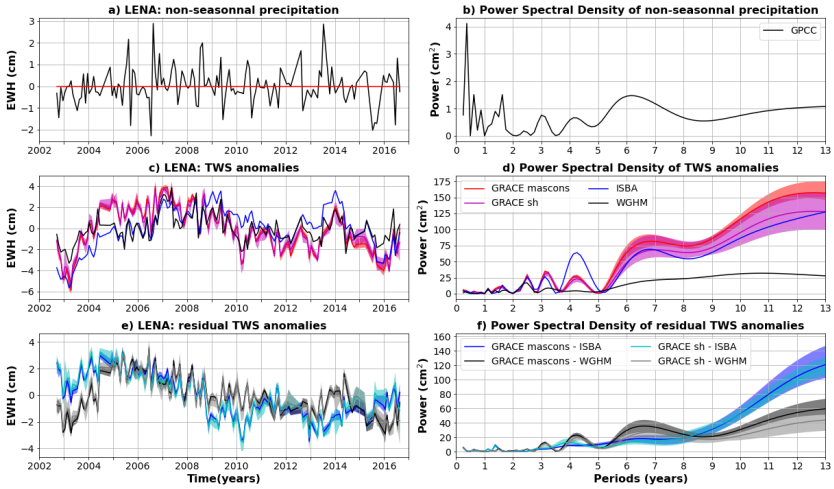

Figure C17: Same as C2 for the Lena basin. Non-seasonal precipitation anomalies are only estimated with GPCC, as a significant part of the river basin is not covered by IMERG satellites due to its high latitude.

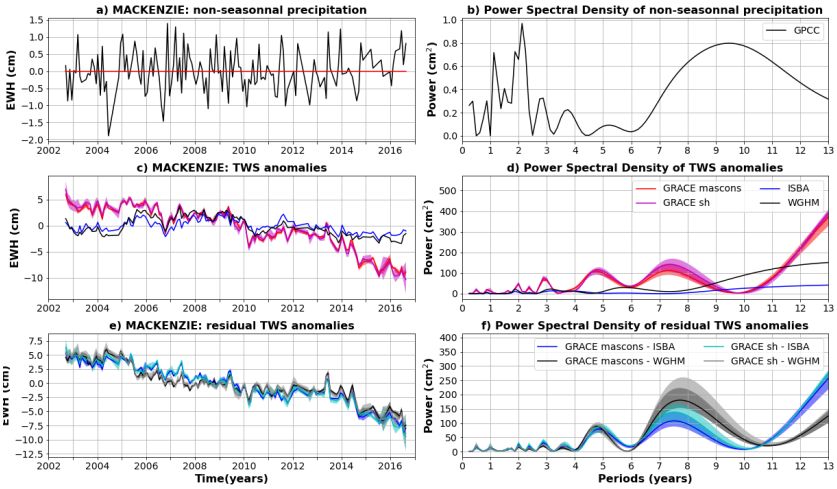

Figure C18: Same as C2 for the Mackenzie basin. Non-seasonal precipitation anomalies are only estimated with GPCC, as a significant part of the river basin is not covered by IMERG satellites due to its high latitude.

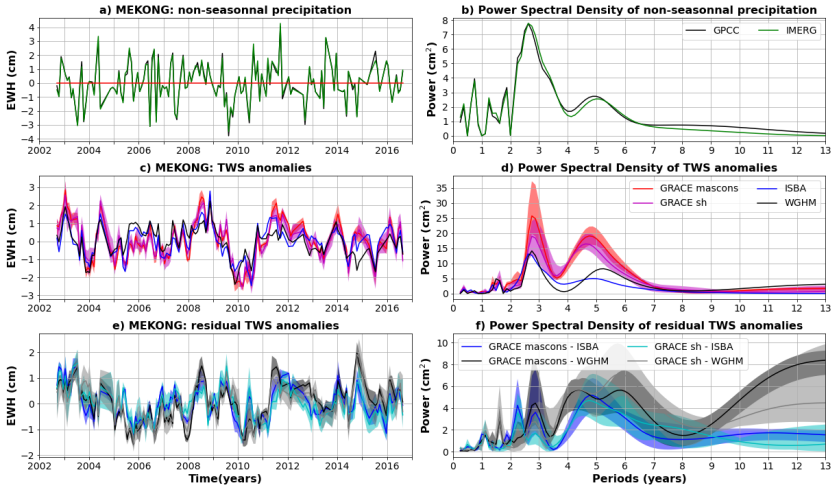

06

07 **Figure C19: Same as C2 for the Mekong basin.**

08

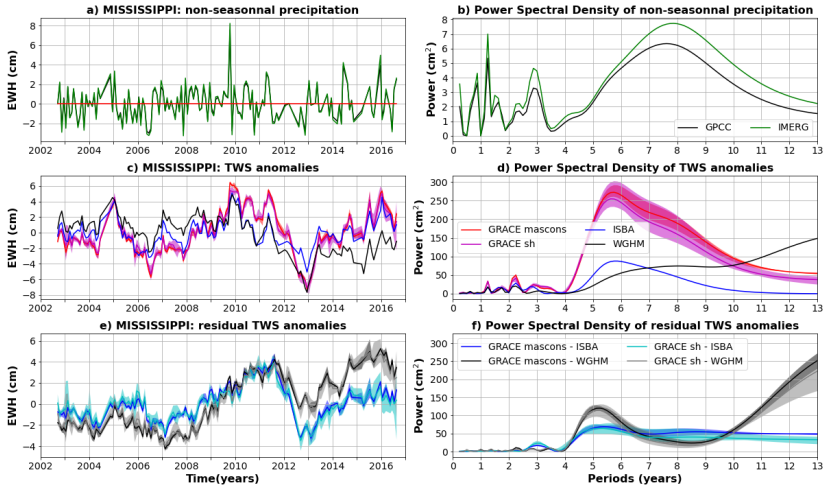

09

10 **Figure C20: Same as C2 for the Mississippi basin.**

11

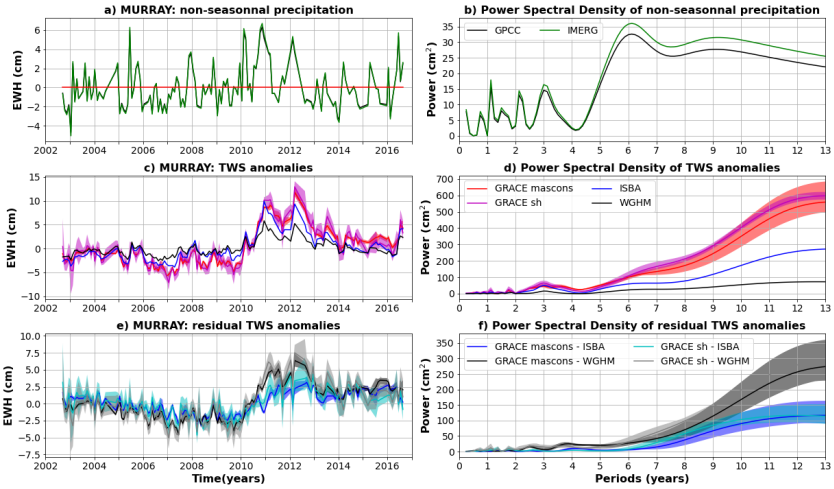

Figure C21: Same as C2 for the Murray basin.

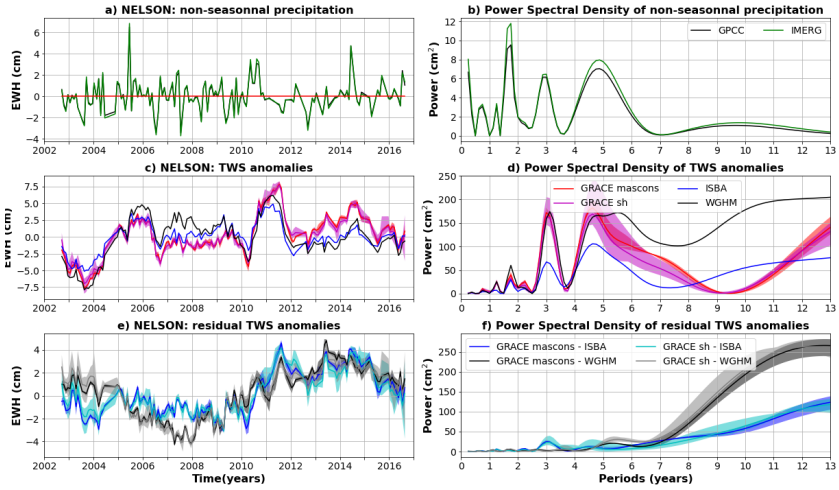

Figure C22: Same as C2 for the Nelson basin.

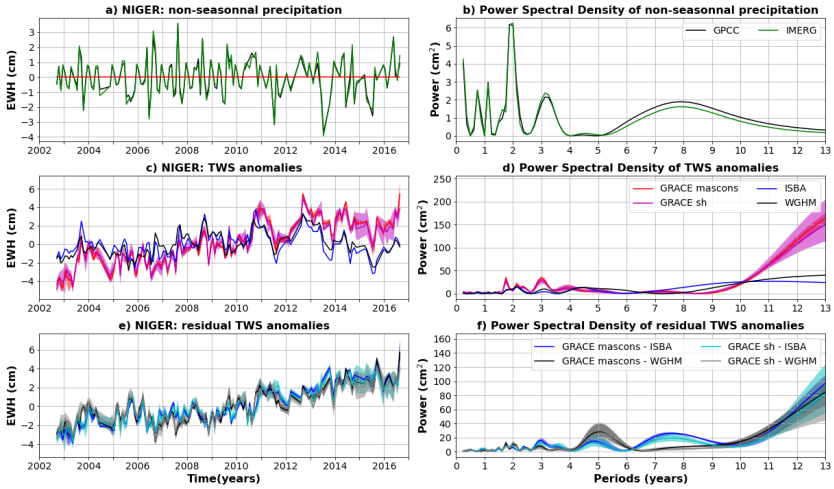

Figure C23: Same as C2 for the Niger basin.

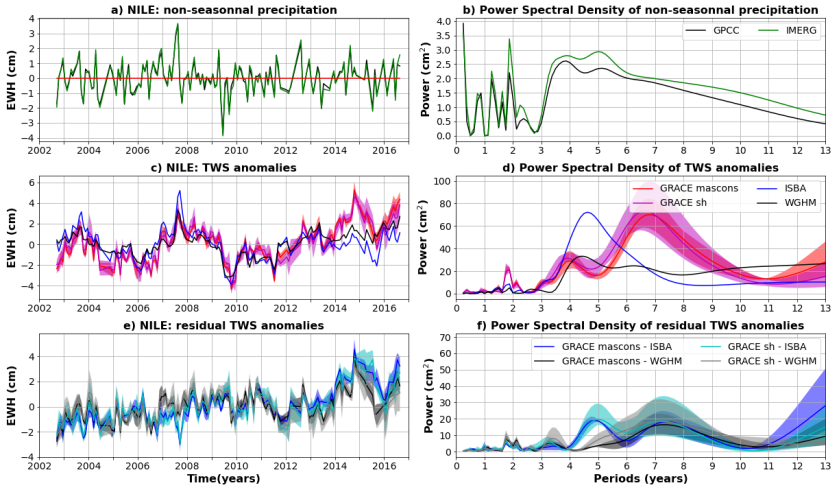

Figure C24: Same as C2 for the Nile basin.

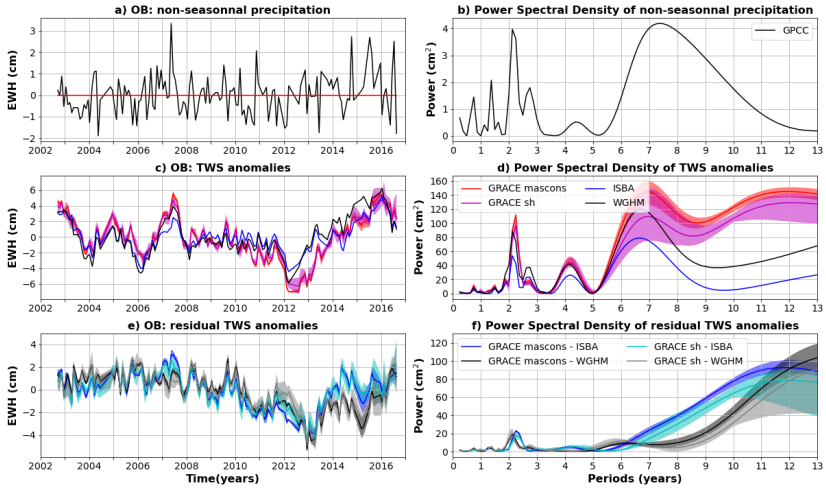

Figure C25: Same as C2 for the Ob basin. Non-seasonal precipitation anomalies are only estimated with GPCC, as a significant part of the river basin is not covered by IMERG satellites due to its high latitude.

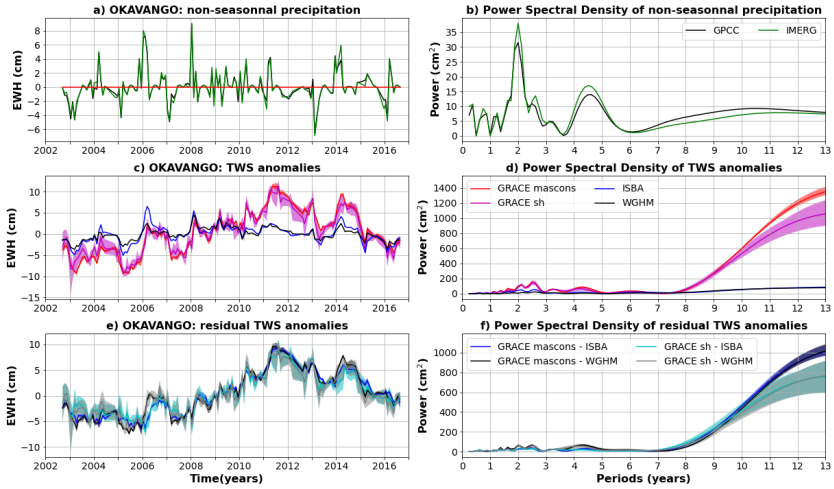

Figure C26: Same as C2 for the Okavango basin.

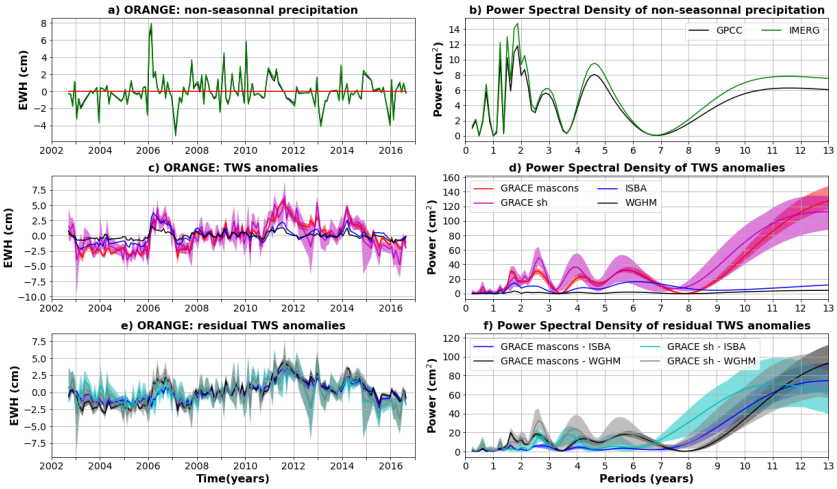

Figure C27: Same as C2 for the Orange basin.

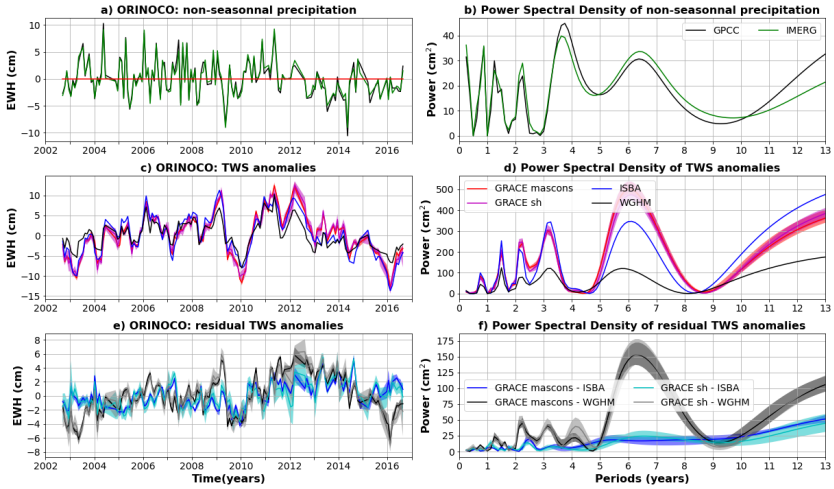

Figure C28: Same as C2 for the Orinoco basin.

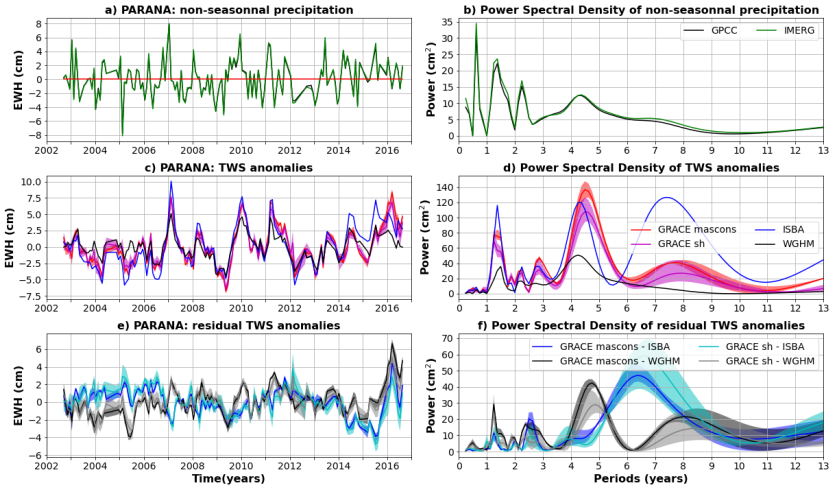

Figure C29: Same as C2 for the Parana basin.

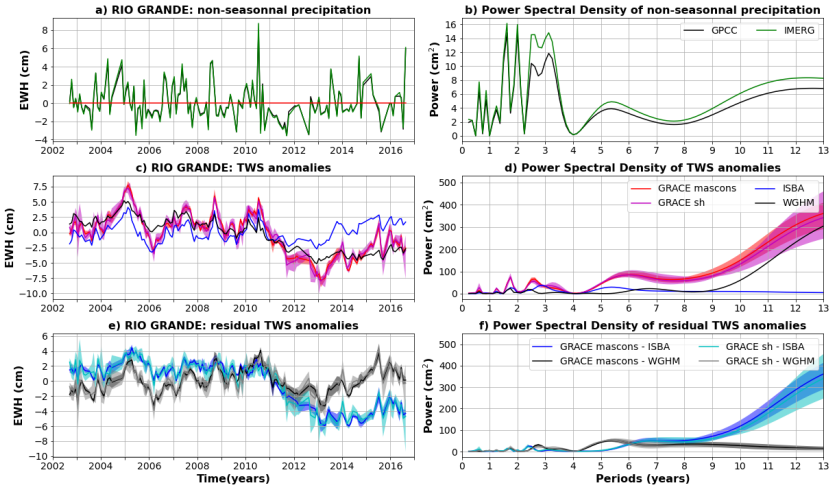

Figure C30: Same as C2 for the Rio Grande basin.

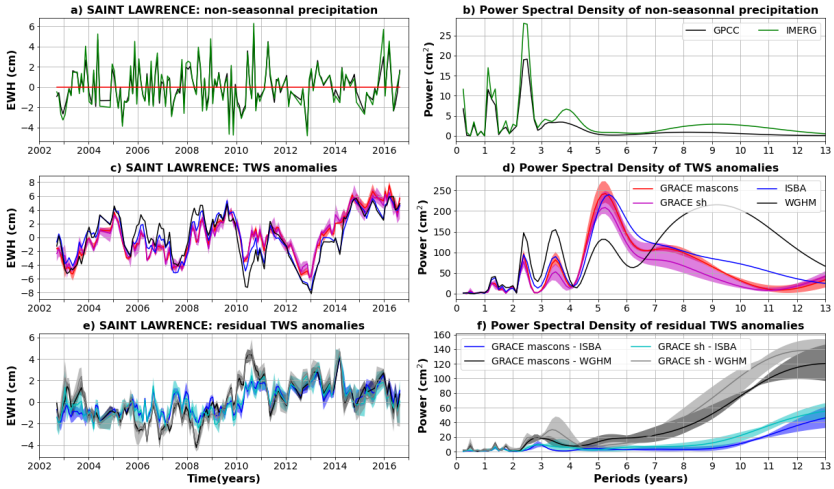

43

44 **Figure C31: Same as C2 for the Saint Lawrence basin.**

45

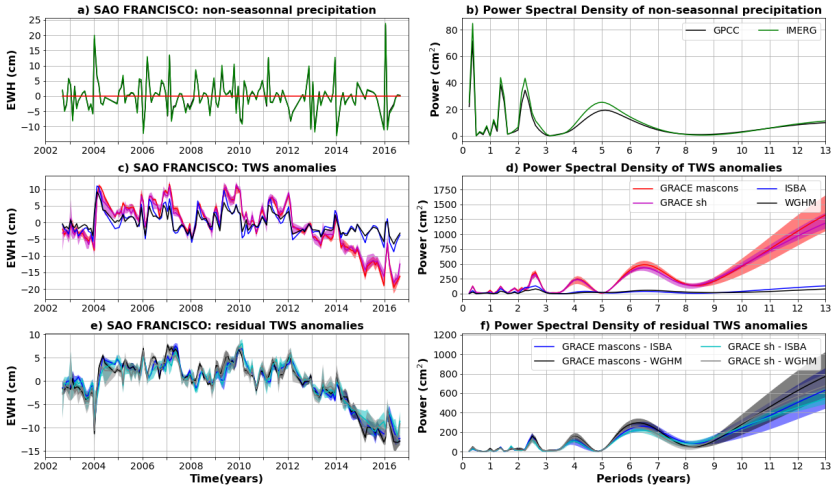

Figure C32: Same as C2 for the Sao Francisco basin.

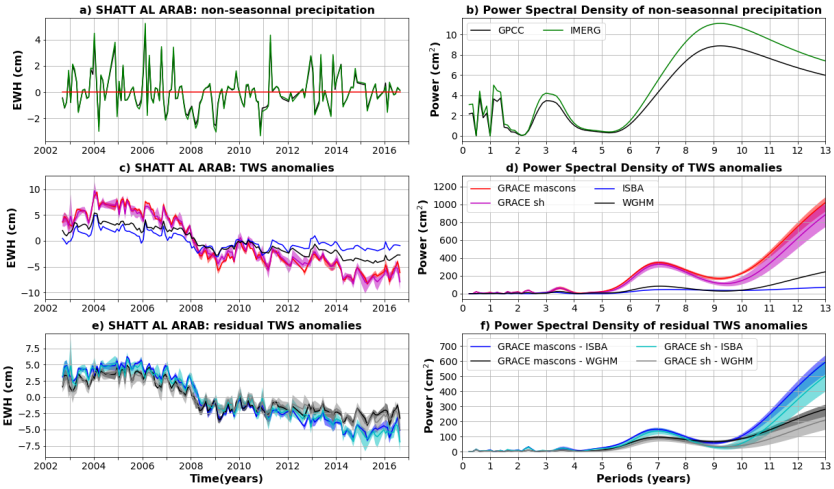

Figure C33: Same as C2 for the Shatt al Arab basin.

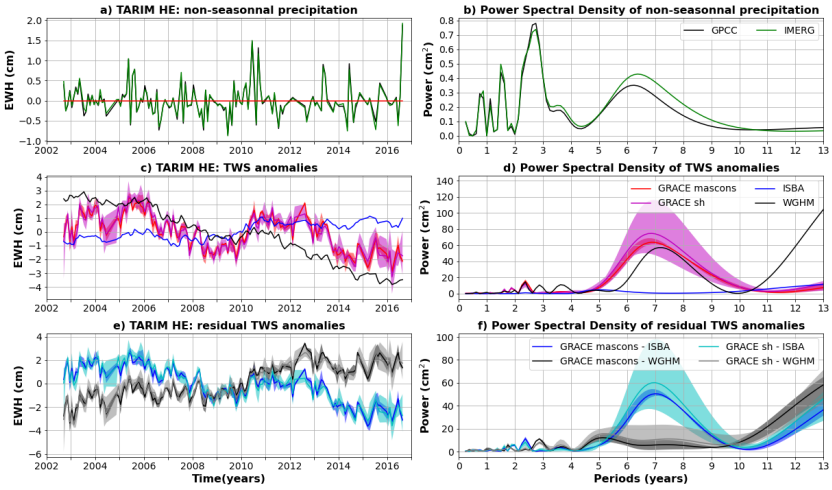

Figure C34: Same as C2 for the Tarim He basin.

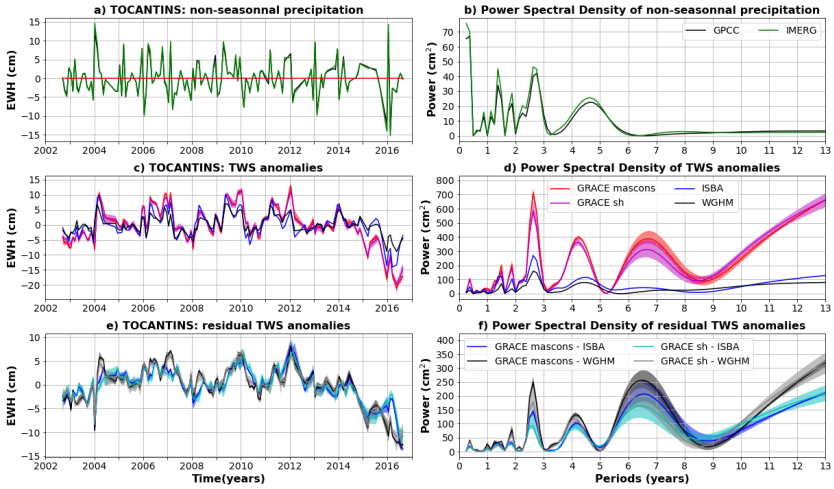

56

57 **Figure C35: Same as C2 for the Tocantins basin.**

58

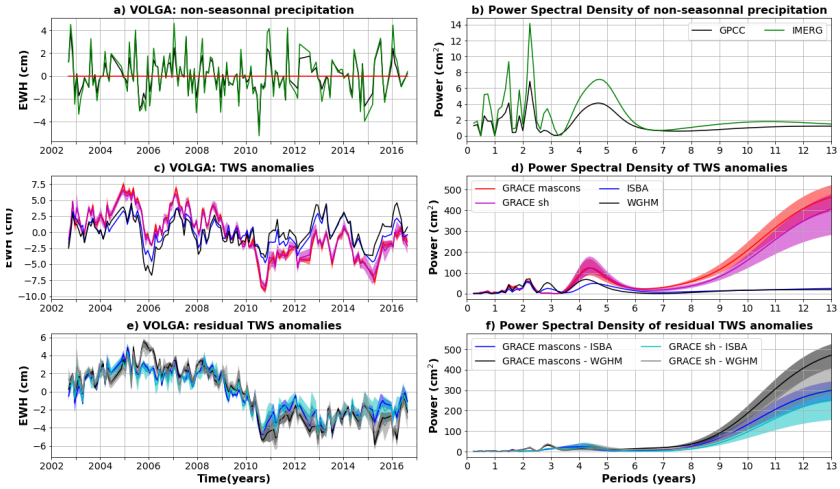

Figure C36: Same as C2 for the Volga basin.

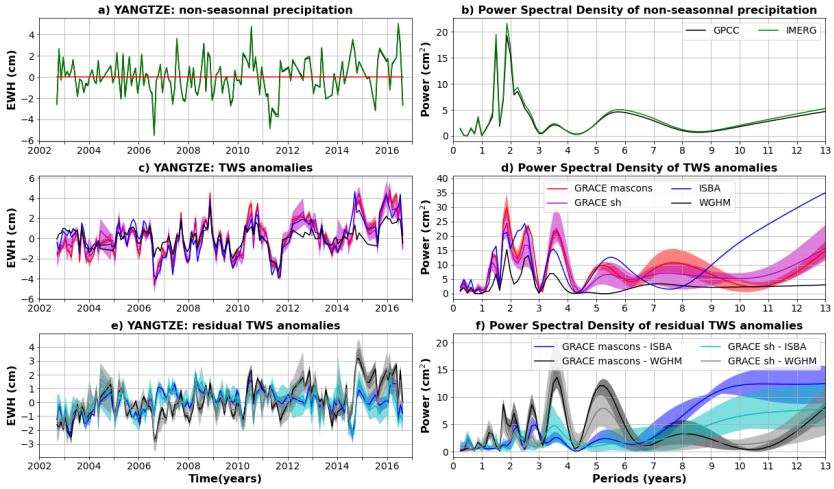

Figure C37: Same as C2 for the Yangtze basin.

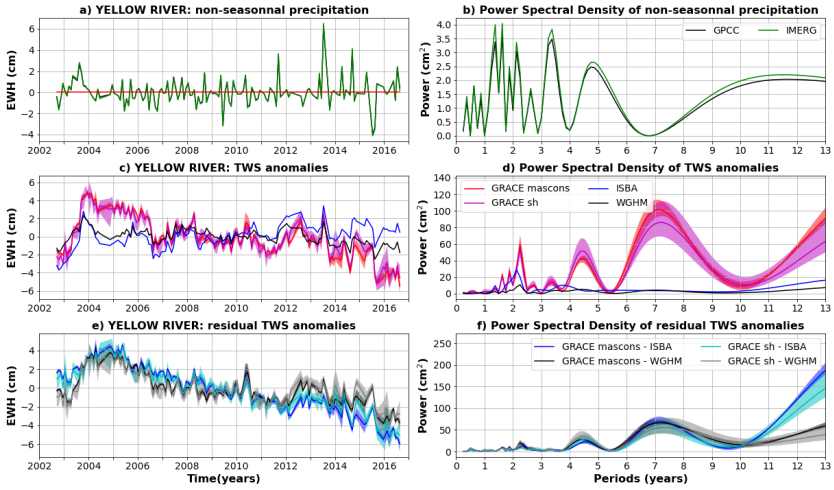

Figure C38: Same as C2 for the Yellow River basin.

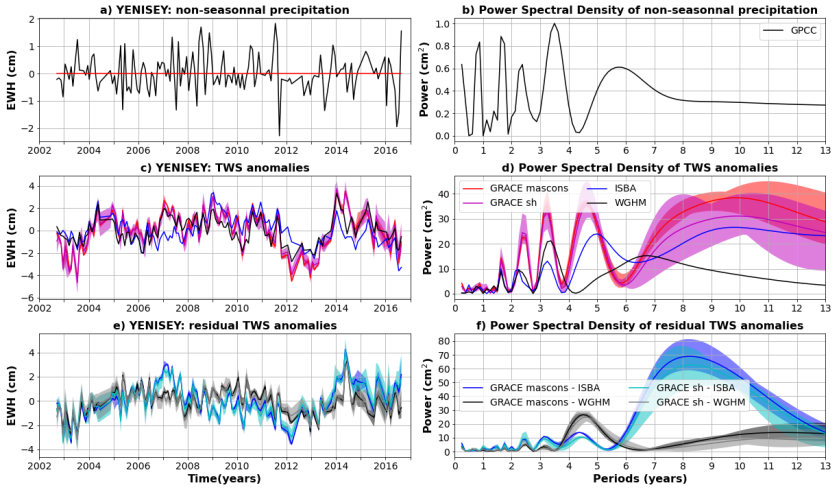

Figure C39: Same as C2 for the Yenisei basin. Non-seasonal precipitation anomalies are only estimated with GPCC, as a significant part of the river basin is not covered by IMERG satellites due to its high latitude.

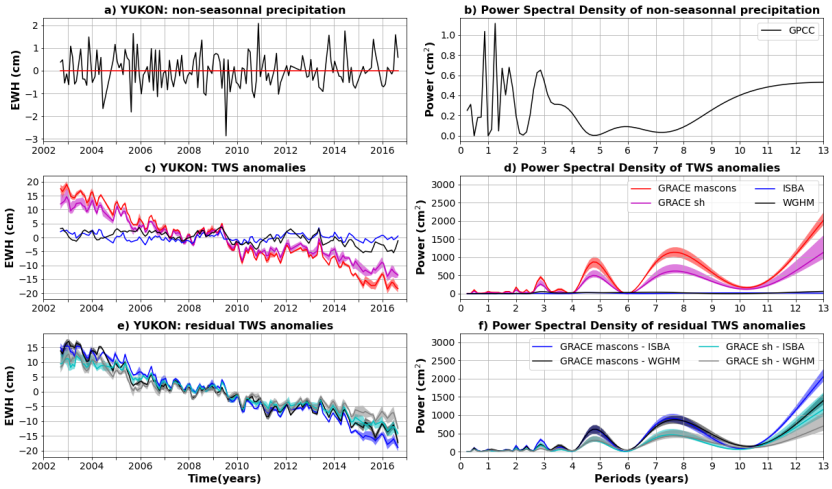

Figure C40: Same as C2 for the Yukon basin. Non-seasonal precipitation anomalies are only estimated with GPCC, as a significant part of the river basin is not covered by IMERG satellites due to its high latitude.

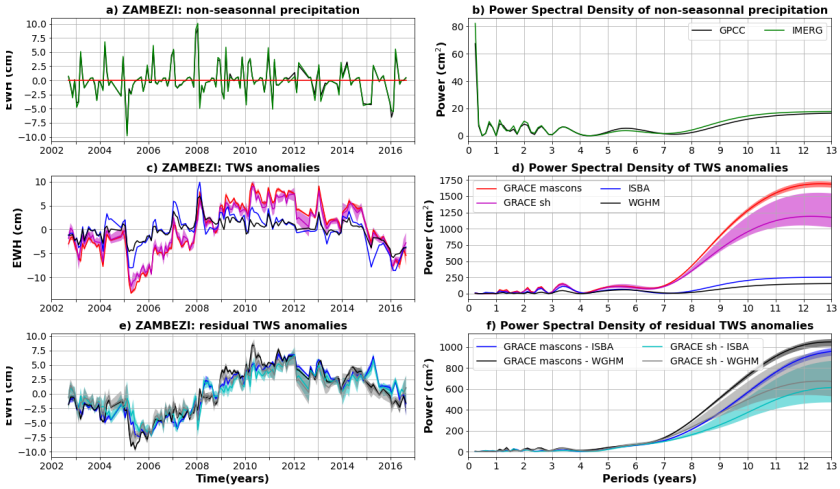

77

78 **Figure C41: Same as C2 for the Zambezi basin**

79

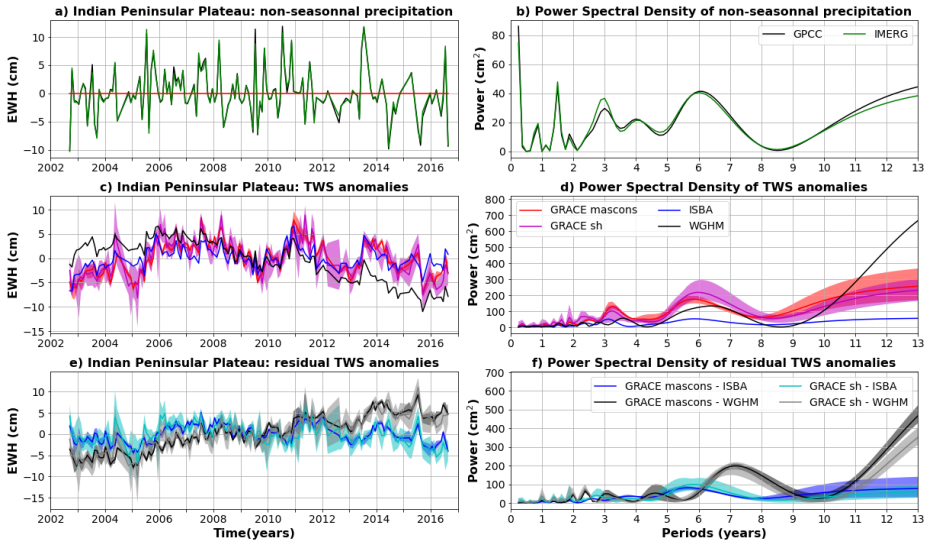

Figure D1 Comparison of TWS and precipitation anomalies averaged across the Indian Peninsular Plateau (latitudes 7 -23°N; longitudes 70-80°E). a) Average precipitation anomalies for the GPCC (gauge-based) and IMERG (satellite-based) products. b) Power Spectral Density (PSD) of average precipitation anomalies. c) TWS anomalies average over the central Amazon for two global hydrological models (ISBA-CTRIP in blue and WGHM in black) and 9 GRACE solutions (mascons in red, spherical harmonic in magenta). The solid line corresponds to the average of the sub-ensemble, the shaded area to the minimum to maximum envelope. d) PSD of the averaged TWS anomalies shown in (c). e) Residual TWS anomalies averaged over the central Amazon corridor and calculated as the difference between GRACE and ISBA-CTRIP (blue when the difference is calculated with mascons, cyan with spherical harmonics) or WGHM (black when the difference is calculated with mascons, grey with spherical harmonics).